



# Aerosol vertical mass flux measurements during heavy aerosol pollution episodes at a rural site and an urban site in the Beijing area of the North China Plain

Renmin Yuan<sup>1</sup>, Xiaoye Zhang<sup>2,4</sup>, Hao Liu<sup>1</sup>, Yu Gui<sup>1</sup>, Bohao Shao<sup>1</sup>, Xiaoping Tao<sup>5</sup>, Yaqiang Wang<sup>2</sup>, Junting Zhong<sup>2</sup>, Yubin Li<sup>3</sup>, and Zhiqiu Gao<sup>3</sup>

<sup>1</sup>School of Earth and Space Sciences, University of Science and Technology of China, Anhui 230026, China

<sup>2</sup>State Key Laboratory of Severe Weather & Key Laboratory of Atmospheric Chemistry of CMA, Chinese Academy of Meteorological Sciences, Beijing 100081, China

<sup>3</sup>School of Geography and Remote Sensing, Nanjing University of Information Science and Technology, Nanjing 210044, China

<sup>4</sup>Center for Excellence in Regional Atmospheric Environment, IUE, CAS, Xiamen 361021, China

<sup>5</sup>School of Physical Sciences, University of Science and Technology of China, Anhui 230026, China

**Correspondence:** Renmin Yuan (rmyuan@ustc.edu.cn) and Xiaoye Zhang (xiaoye@cma.gov.cn)

Received: 5 December 2018 – Discussion started: 10 April 2019

Revised: 29 June 2019 – Accepted: 15 September 2019 – Published: 16 October 2019

**Abstract.** Due to excessive anthropogenic emissions, heavy aerosol pollution episodes (HPEs) often occur during winter in the Beijing–Tianjin–Hebei (BTH) area of the North China Plain. Extensive observational studies have been carried out to understand the causes of HPEs; however, few measurements of vertical aerosol fluxes exist, despite them being the key to understanding vertical aerosol mixing, specifically during weak turbulence stages in HPEs. In the winter of 2016 and the spring of 2017 aerosol vertical mass fluxes were measured by combining large aperture scintillometer (LAS) observations, surface PM<sub>2.5</sub> and PM<sub>10</sub> mass concentrations, and meteorological observations, including temperature, relative humidity (RH), and visibility, at a rural site in Gucheng (GC), Hebei Province, and an urban site at the Chinese Academy of Meteorological Sciences (CAMS) in Beijing located 100 km to the northeast. These are based on the light propagation theory and surface-layer similarity theory. The near-ground aerosol mass flux was generally lower in winter than in spring and weaker in rural GC than in urban Beijing. This finding provides direct observational evidence for a weakened turbulence intensity and low vertical aerosol fluxes in winter and polluted areas such as GC. The HPEs included a transport stage (TS), an accumulative stage (AS), and a removal stage (RS). During the HPEs from 25 to 31 January 2017, in Beijing, the mean mass flux decreased by 51 %

from 0.0049 mg m<sup>−2</sup> s<sup>−1</sup> in RSs to 0.0024 mg m<sup>−2</sup> s<sup>−1</sup> in the TSs. During the ASs, the mean mass flux decreased further to 0.00087 mg m<sup>−2</sup> s<sup>−1</sup>, accounting for approximately one-third of the flux in the TSs. A similar reduction from the TSs to ASs was observed in the HPE from 16 to 22 December 2016 in GC. It can be seen that from the TS to the AS, the aerosol vertical turbulent flux decreased, but the aerosol particle concentration within the surface layer increased, and it is inferred that in addition to the contribution of regional transport from upwind areas during the TS, suppression of vertical turbulence mixing confining aerosols to a shallow boundary layer increased accumulation.

## 1 Introduction

Recently, due to the country's rapid development of industrialization and urbanization, China has experienced heavy aerosol pollution episodes, particularly in the Beijing, Tianjin, and Hebei (BTH) region, which is one of the most polluted areas in China (Zhang et al., 2012). The pollution episodes often last for a long duration in the BTH region and cover a wide area, particularly in winter; they also severely reduce near-ground visibility (Lei and Wuebbles, 2013) and

can have detrimental effects on public health (He et al., 2018; Cao et al., 2012). This heavily polluted environment has received extensive attention in recent years, and many observational studies have been carried out (Zhong et al., 2018b; Sun et al., 2014; Wang et al., 2015; Guo et al., 2011; X. Y. Zhang et al., 2009; Huang et al., 2014). Modelling studies have also been performed to examine the regional transport of pollutants (Wang et al., 2014) and to study the important role of large-eddy convective turbulent mixing in the vertical transfer of pollutants from a field campaign in Beijing (Li et al., 2018). However, few studies on the turbulence contribution of the aerosol turbulent flux in the surface layer have been conducted.

Ground pollutant emissions are known as the main source of aerosols in the atmosphere. However, in previous studies, no measurements of ground emissions during heavy pollution events were collected. Surface emission data are currently required for model verification and pollution predictions, and these data are primarily obtained through emission inventories (Wu et al., 2012; Bond et al., 2004). The establishment of emission inventories is primarily based on emission activity and emission factor (EF) data (Akagi et al., 2011; Lu et al., 2011; Roden et al., 2006; Zhang and Tao, 2009). Emissions data are mainly obtained from statistical yearbooks (Q. Zhang et al., 2009). Some studies have used fixed EFs while others have implemented dynamic EFs (Bond et al., 2004; Q. Zhang et al., 2009). Many factors are considered in dynamic EFs, such as the size of a city, the degree of economic development, the type of fuel, the kind of technology, product energy consumption, the control technology, and so on, as well as estimates based on actual measured meteorological parameters and aerosol parameters (Chen et al., 2015; Karvosenoja et al., 2008; Shen et al., 2013). A numerical model has also been used to estimate average fleet emission factors in typical urban conditions (Ketzel et al., 2003; Krecl et al., 2018). The uncertainties in the emissions of primary aerosols for inventories are high due to the highly uncertain contributions from the residential sector (Li et al., 2017), and the error in aerosol fluxes based on the use of emission inventories is huge (Liu et al., 2017; Zheng et al., 2017). Emission inventories constructed using the EF method provide only the total emission amount of atmospheric pollutants within a region. However, the emission data should be gridded to a suitable scale for air quality modelling and pollution predictions. Thus, near-surface aerosol emission data with a higher temporal and spatial resolution are urgently needed.

Many methods have been used to obtain aerosol flux data. For the upward transport of aerosols near the surface layer, the aerodynamic approach was adopted in the early years. The aerosol concentration gradient at different heights was measured and then calculated based on the similarity theory of the near-surface layer or calculated by the boundary layer box model, which can be based on meteorological data (Ceburnis et al., 2016; Hourdin et al., 2015; Zhang and Li, 2014).

The emission rates of bioaerosols were also estimated from spore counts and molecular tracers (Elbert et al., 2007). The abundance of microbes and meteorological data were measured, and an estimate may be derived from the sea–air exchange of microorganisms (Mayol et al., 2014).

With the use of instruments for measuring the number of aerosol particles (for example, a condensational particle counter, abbreviated as CPC by TSI), the eddy covariance (EC) method has been applied, and measurement of the aerosol particle number flux has become possible (Buzorius et al., 1998). The vertical turbulent flux of the aerosol particle number density  $F_p$  is denoted as a cross-covariance between the aerosol particle number concentration  $N'$  and the vertical wind speed  $w'$  (Ripamonti et al., 2013). To obtain vertical turbulent flux of the aerosol number density, the EC principle allows the number flux from fluctuation measurements to be quantified. As a result, the vertical turbulent flux of the aerosol particle number density has been measured in many cities, such as in Toronto, Canada (Gordon et al., 2011); Stockholm, Sweden (Vogt et al., 2011b); Helsinki, Finland (Ripamonti et al., 2013), London, UK (Harrison et al., 2012); and the Blodgett Forest Observatory in the United States (Farmer et al., 2011), and sea salt aerosol fluxes have been measured in northern Europe (Brooks et al., 2009; Sproson et al., 2013). These results have shown the quantitative relationship among urban aerosol fluxes, urban vehicle emissions, and meteorological conditions (Järvi et al., 2009) and have been used to determine transport characteristics of sea salt aerosol and provide further knowledge of aerosol properties (Nemitz et al., 2009). These measurements have been mainly collected in cities because of their anthropogenic contributions to aerosol emissions. These data can be used as routine model inputs. Direct eddy covariance measurements of aerosol exchanges in tropical forests, where primary biological aerosol particles represent a substantial fraction of the airborne particulate matter (Graham et al., 2003), were also performed by Ahlm et al. (2010a, b) and Whitehead et al. (2010), potentially giving a proxy for microbial emissions in tropical ecosystems.

Although measurements of urban aerosol particle number density fluxes have been collected, the current eddy covariance method only provides fluxes for the aerosol particle number density at a certain point. We know that the underlying surface of a city is very complex, and thus the aerosol particle flux is not homogeneous in the horizontal. For a complex underlying surface such as a city, these point measurements are not representative of wider area. Therefore, it is of great importance to design an aerosol flux measurement system with larger spatial representation.

The use of eddy covariance principles to measure sensible heat fluxes has been widely performed (Lee, 2004). Current sensible heat fluxes can also be obtained using a large aperture scintillometer (LAS) based on the light propagation theory and atmospheric surface layer similarity theory (Zeweldi et al., 2010). This configuration makes it possible

to achieve aerosol mass flux measurements using the same principles. Recently, we measured the imaginary part of the atmospheric equivalent refractive index structure parameter based on the light propagation theory (Yuan et al., 2015). The results showed that the imaginary part of the atmospheric equivalent refractive index structure parameter is related to turbulent transport and the spatial distribution characteristics of aerosols. Experiments also showed that there is a strong correlation between the imaginary part of the atmospheric equivalent refractive index and the mass concentration of aerosol particles (Yuan et al., 2016). Thus, similar to the temperature structure parameter reflecting the sensible heat flux, the structural parameter of the imaginary part of the atmospheric equivalent refractive index can reveal the mass flux of aerosol particles. This paper attempts to measure the aerosol mass flux in the BTH area, especially during heavy aerosol pollution episodes.

Generally, based on the  $\text{PM}_{2.5}$  daily mean mass concentration limit in the primary standard of China's national environmental quality standards (EPD, 2012), a pollution episode is referred to as the period during which the  $\text{PM}_{2.5}$  concentration exceeds  $80\text{ }\mu\text{g m}^{-3}$  for 3 consecutive days between two clean periods, while a period during which the  $\text{PM}_{2.5}$  level is less than  $35\text{ }\mu\text{g m}^{-3}$  is defined as a clean period. Pollution episodes with peak  $\text{PM}_{2.5}$  values of more than  $400\text{ }\mu\text{g m}^{-3}$  or less than  $300\text{ }\mu\text{g m}^{-3}$  are termed heavy-pollution episodes (HPEs) or light-pollution episodes (LPEs), respectively (Zhong et al., 2017b).

To gain a deeper understanding of the interaction between atmospheric heavy pollution and weather in the BTH region, joint observations have been carried out in the BTH region since the winter of 2016 (Zhong et al., 2018b, c; Wang et al., 2018; Shen et al., 2018). Based on meteorological causes of the increase or decrease in  $\text{PM}_{2.5}$  mass concentrations, an HPE in the BTH region can be divided into a transport stage (TS), an accumulative stage (AS), and a removal stage (RS). During the TS, the  $\text{PM}_{2.5}$  high concentration levels are caused by relatively strong southerly winds, which carry polluted air masses from more populated southern industrial regions (Guo et al., 2014; Zhong et al., 2018a). Before elevation of  $\text{PM}_{2.5}$  concentrations during TSs, the urban  $\text{PM}_{2.5}$  mass concentration of Baoding, which is typically representative of pollution conditions in the south of Beijing, was much higher than Beijing; the winds in Beijing rapidly shifted from northerly to southerly. Then the rising in  $\text{PM}_{2.5}$  occurred, consistently with southerly slight or gentle breezes in the boundary layer (BL). The southerly air mass moves more than  $288\text{ km d}^{-1}$  below 500 m (estimated from the measured wind speed), which are fast enough to transport pollutants to Beijing. Such processes indicate southerly pollutant transport is primarily responsible for elevation of  $\text{PM}_{2.5}$  concentrations, given the pollution transport pathway of the southwest wind belt determined by the unique geographic features of the North China Plain, with the Taihang Shan and the Yan Shan strengthening the southwest wind belt

and leading the convergence of pollutant transport in Beijing (Su et al., 2004). During the ASs,  $\text{PM}_{2.5}$  increase is dominated by stable atmospheric stratification characteristic of southerly slight or calm winds, near-ground anomalous inversion, and moisture accumulation. When aerosol particles are accumulated by vertical transport to a certain degree, the dominant scattering aerosols will substantially back-scatter solar radiation, causing a reduction in the amount of solar radiation that reaches the surface, which creates a near-ground cooling effect resulting in the lack of vertical mixing in the near-surface layer (Zhong et al., 2018c). A feedback effect of further worsened meteorological conditions aggravates  $\text{PM}_{2.5}$  pollution (Zhong et al., 2017a). During the RSs, strong north-westerly winds whose velocity increases with height occur predominantly. Strong northerly winds are from less populated north mountainous areas and carry unpolluted air masses to Beijing, which is favourable for pollution dispersion. The observations reveal the large-scale and mesoscale transport processes of aerosols between HPEs in the BTH region in the winter of 2016. However no research on quantifying the contribution of surface emissions to the concentration of pollutants has been conducted in the BTH area during HPEs. In this study, we focus on aerosol emission during HPEs through field observations of aerosol turbulent based on the light propagation theory and surface similarity in the Beijing urban district and Gucheng suburban area.

The second section of this paper introduces the theory of aerosol vertical turbulent flux measurements, the third section introduces the experiment, the fourth section gives the experimental results, and, finally, the conclusion and discussion are presented in the fifth section.

## 2 Theory and methods

The principles for calculating the vertical flux of aerosol particles and the approach for calculating the friction velocity and characteristic temperature using the temperature and wind profiles is presented in the following subsections.

### 2.1 Calculation of the aerosol mass vertical flux

According to the micrometeorological principle (Stull, 1988), similar to the estimation method of the sensible heat flux, the aerosol flux  $F_a$  can be obtained as follows:

$$F_a = u_* M_*, \quad (1)$$

where  $u_*$  is the friction velocity, which can be obtained from the temperature and wind speed profiles or directly from three-dimensional wind speed measurements; see Sect. 2.2. Prior experiments have shown that the spectral characteristics of aerosol number concentration fluctuations approximate the spectral characteristics of molecular density fluctuations (Mårtensson et al., 2006; Vogt et al., 2011b). Therefore, aerosol particles can be approximated as scalars for turbulent statistics, and characteristic parameters  $M_*$  similar to the

scalars can be introduced, which can be regarded as the atmospheric aerosol mass concentration scale in the surface layer and deduced from surface layer similarity theory. This approximation is similar to the surface-layer temperature scale (Stull, 1988) as follows:

$$\frac{C_M^2(z-d)^{2/3}}{M_*^2} = \eta(\xi), \quad (2)$$

where  $z$  is the measurement height,  $d$  is the zero-displacement height (Evans and De Bruin, 2011; Hartogensis et al., 2003),  $\xi = (z-d)/L$  is the nondimensional stability parameter,  $L$  is the Monin–Obukhov (MO) length and defined as  $L = \frac{\bar{T} u_*^2}{\kappa g T_*}$  (Stull, 1988),  $\bar{T}$  is the average temperature,  $T_*$  is the surface-layer characteristic temperature,  $\kappa$  is the von Karman constant, which is 0.4, and  $g$  is acceleration due to gravity. The stability function ( $\eta(\xi)$ ) can be expressed as follows depending on the stability condition (DeBruin et al., 1995):

$$\eta(\xi) = a_1 [1 - a_2 \xi]^{-2/3} \quad (3)$$

for unstable conditions ( $\xi < 0$ ), and

$$\eta(\xi) = b_1 [1 + b_2 (\xi)^{e_1}] \quad (4)$$

for stable conditions ( $\xi > 0$ ) (Wyngaard et al., 1971).

In Eqs. (3) and (4),  $a_1$ ,  $a_2$ ,  $b_1$ ,  $b_2$ , and  $e_1$  are constants, and different experiments have provided different values, although the differences between these results are small. It is assumed that the aerosol mass concentration fluctuation characteristics are the same as the temperature fluctuation characteristics and the same similarity law of Eq. (2) is satisfied. Therefore, based on the experimental data, the values

of  $\sqrt{\frac{C_M^2(z-d)^{2/3}}{\eta(\xi)}}$  and  $T_*$  are calculated using various schemes. After comparing the differences between the two, the scheme of DeBruin et al. (1995) with  $a_1 = 4.9$ ,  $a_2 = 9$ ,  $b_1 = 5$ , and  $b_2 = 0$  is taken based on minimal difference using the experimental data of this study.

$C_M^2$  in Eq. (2) is the aerosol mass concentration structure parameter. We assume that the aerosol particles in the atmosphere follow the movement of the air and satisfy the turbulent motion law. Previous studies have shown that the particle concentration fluctuation spectra follow a “ $-5/3$ ” power law under unstable stratification conditions (Mårtensson et al., 2006; Vogt et al., 2011b), and the velocity–concentration co-spectra follows a “ $-4/3$ ” power law (Mårtensson et al., 2006; Vogt et al., 2011a; Kaimal et al., 1972). Thus, similarity of atmospheric aerosols and temperature can be assumed for the purpose. Then, at a separation ( $r$ ) of the order in the inertial subrange in a locally isotropic field, the aerosol mass concentration (denoted as  $M_a$ ) structure function ( $D_M(r)$ ) follows a “ $2/3$ ” law (Wyngaard, 2010) and can be expressed as  $D_M(r) = \overline{[M_a(x) - M_a(x+r)]^2} = C_M^2 r^{2/3}$ , where  $x$  is the position vector,  $r$  is the separation vector, and the overbar indicates the spatial average.

The following describes the method to deduce the aerosol mass concentration structure parameter  $C_M^2$ .

Although the aerosol particles are dispersed in the air, the macroscopic behaviour of the gas-particle two-phase mixture is the same as if it is perfectly continuous in structure and physical quantities, such as the mass and refractive index associated with the matter contained within a given small volume, which will be regarded as being spread continuously over that volume. The aerosol particles and gases in the atmosphere can be considered as an equivalent medium, and an atmospheric equivalent refractive index (AERI)  $n_{\text{equ}}$  is introduced that contains the real part  $n_{\text{re}}$  and the imaginary part  $n_{\text{im}}$  of the equivalent refractive index. Thus,  $n_{\text{equ}} = n_{\text{re}} + i \cdot n_{\text{im}}$ . For visible light, the attenuation of light by gases in the atmosphere is very weak; the cause of the attenuation is the absorption and scattering due to aerosol particles. Therefore, the real part of the equivalent medium of aerosol particles and gases is determined by the gas composition of the air. The fluctuation of the real part is mainly determined by temperature fluctuations; the imaginary part is determined by the aerosol particles, and the fluctuation of the imaginary part is determined by fluctuations in the aerosol concentration.

For visible light, there is a robust linear relationship between the variation of the real part of the AERI and the variation of the atmospheric temperature, namely,  $R_{\text{TN}} = \frac{\delta T}{\delta n_{\text{re}}}$ ; thus, we have the following:

$$R_{\text{TN}} = -1.29 \times 10^4 \times \left(1 + \frac{7.52 \times 10^{-3}}{\lambda^2}\right)^{-1} \frac{\bar{T}}{\bar{P}}, \quad (5)$$

which is based on the relationship between the real part of the AERI ( $n_{\text{re}}$ ) and atmospheric temperature (Tatarskii, 1961). Because the wavelength is deterministic, the ratio  $R_{\text{TN}}$  can be obtained by measuring the atmospheric temperature. The imaginary part of the AERI ( $n_{\text{im}}$ ) has a close correspondence with the extinction coefficient of the equivalent medium, and the extinction coefficient is inversely proportional to the visibility. The light wavelength is selected as  $0.620 \mu\text{m}$ . This wavelength is only weakly absorbed by  $\text{O}_3$ ; therefore, the observed absorption is primarily due to aerosol (Brion et al., 1998; Lou et al., 2014; Nebuloni, 2005). Higher concentrations of aerosols in the atmosphere are related to lower visibility and vice versa; thus, the relationship between the imaginary part of the AERI and the atmospheric aerosol mass concentration can be established. The ratio of the atmospheric aerosol mass concentration to the imaginary part of the AERI  $R_{\text{MN}}$  can be defined as follows:

$$R_{\text{MN}} = \frac{M_a}{n_{\text{im}}}. \quad (6)$$

Theoretical analysis has revealed that  $R_{\text{MN}}$  is associated with the aerosol particle size distribution, mass density of the aerosol particles, and the aerosol particle refractive index. Because of the relatively small variations in particle size distributions and aerosol refractive index (Dubovik et al., 2002),

$R_{MN}$  can be treated as a constant for surface-layer aerosols at a given location. Of course,  $R_{MN}$  can be obtained by simultaneously measuring  $M_a$  and the imaginary part of the AERI, so that real-time  $R_{MN}$  can be obtained.  $M_a$  approximates the  $PM_{10}$  value. The variable  $n_{im}$  can be calculated as follows (Yuan et al., 2016):

$$n_{im} = \frac{0.55e - 6}{4\pi} \cdot \frac{3.912}{L_V}, \quad (7)$$

where the unit of visibility ( $L_V$ ) is metres.

According to Eqs. (5) and (6), we have the following:

$$C_T^2 = R_{TN}^2 C_{n,Re}^2, \quad (8)$$

$$C_M^2 = R_{MN}^2 C_{n,Im}^2, \quad (9)$$

Thus, the temperature structure parameter  $C_T^2$  and the aerosol mass concentration fluctuation structure parameter  $C_M^2$  are converted into the measurement of the real and imaginary structural parameters of the AERI, namely  $C_{n,Re}^2$  and  $C_{n,Im}^2$ , respectively.

The measurement of relevant parameters is performed based on the light propagation theory. When light is transmitted in an equivalent medium, the AERI fluctuation will cause light fluctuations in light intensity. When the attenuation caused by scattering and absorption along the propagation path is very weak, light intensity fluctuation depends on the fluctuation of the real part of the AERI along the propagation path. When the attenuation caused by scattering and absorption along the propagation path is relatively strong, the light intensity fluctuation is also related to the fluctuation of the imaginary part of the AERI along the propagation path. With the spectral analysis method, the LAS light intensity fluctuations can be separated into the contributions of the real and imaginary parts of the AERI. The contribution of the real part of the AERI corresponds to the high frequencies, whereas the contribution of the imaginary part of the AERI corresponds to the low frequencies, suggesting that the variances resulting from the real and imaginary parts are independent. Therefore, the light intensity variances induced by the real and imaginary parts can be detected separately at high frequencies and low frequencies from the LAS measurements (Yuan et al., 2015). Thus, the real and imaginary structure parameters of the AERI can be calculated by our developed LAS.

So far, we have completed the estimation of the aerosol mass turbulent flux.

According to the previous derivation and analysis, there are two calculation schemes for determining the aerosol mass

flux:

$$F_{a1} = \left( \frac{C_{n,Im}^2}{C_{n,Re}^2} \right)^{1/2} \frac{R_{MN}}{R_{TN}} u_* |T_*|, \quad (10)$$

$$F_{a2} = u_* \sqrt{\frac{C_M^2 (z-d)^{2/3}}{\eta(\xi)}} = u_* R_{MN} \sqrt{\frac{C_{n,Im}^2 (z-d)^{2/3}}{\eta(\xi)}}. \quad (11)$$

When the free convection approximation ( $-\xi \gg 1$ ) is assumed, based on the definition of the MO length, and the similarity theory (Wyngaard et al., 1971), the following can be obtained:

$$F_{a3} = a \left( \frac{g}{T} \right)^{1/2} R_{TN}^{1/2} (C_{n,Re}^2)^{1/4} R_{MN} (C_{n,Im}^2)^{1/2} (z-d), \quad (12)$$

where the coefficient  $a = a_1^{-3/4} a_2^{1/2} \kappa^{1/2}$  can be taken as 0.567 (DeBruin et al., 1995; Lagouarde et al., 2006). Equations (10)–(12) are the theoretical basis for the aerosol mass flux measurements.

According to Eqs. (10)–(12), the vertical turbulent flux of aerosol particles is related to the strength of turbulent fluctuations of temperature and aerosol mass concentration fluctuations.

In this study, data from a weather tower in the north of Beijing were used. The weather tower is 6.1 km far from the CAMS site. The meteorological observation data from the weather tower show that applicability of the Monin–Oubhov similarity theory under stable conditions causes a significant error for  $T^*$  or  $u_*$ , while the Monin–Oubhov similarity theory is still basically applicable in the case of unstable stratification (Liu et al., 2009). In the roughness sub-layers of other cities, under the condition of unstable stratification, the local similarity theory is similar to MOST (Zou et al., 2015, 2018). Because the height of the LAS instrument at the CAMS site was 43 m, during most of the time the conditions assumed for free convection were easily satisfied. During the day, the surface layer is usually unstable. At night, for the city, even if there is an inversion at a higher altitude, due to the existence of the urban heat island, the surface layer is often weakly unstable. The stable stratification situation is rare (Li et al., 2007). Therefore, aerosol fluxes in Beijing are calculated using Eq. (12) based on the assumption of free convection.

Based on the discussion above, the LAS technique is capable of determining the magnitude of the flux but not the sign. In general, the aerosols are very heterogeneous in space and the measured fluxes typically show large variation in magnitude, including the sign. Over the polluted areas, which behave as the source, the emissions presumably overwhelmingly exceed the deposition sinks (Ripamonti et al., 2013). Therefore, a rough quantification of the deposition sink would allow the conclusion that the sink term is negligible and the flux quantified by LAS can be assumed to represent the upward fluxes.

## 2.2 Calculation of the friction velocity and surface-layer characteristic temperature

To calculate the aerosol vertical turbulent flux, according to Eq. (10), the values of the friction velocity  $u_*$  and the characteristic temperature  $T_*$  are required. These can be obtained via wind speed and temperature profile data. From the near-surface similarity theory, the temperature and wind speed data measured at two heights of  $z_1$  and  $z_2$  can be used in the expressions of the friction velocity  $u_*$  and the characteristic temperature  $T_*$  (Stull, 1988) as follows:

$$u_* = \frac{\kappa [U(z_2) - U(z_1)]}{\ln \frac{z_2}{z_1} - \Psi_U(\xi_2) + \Psi_U(\xi_1)}, \quad (13)$$

$$T_* = \frac{\kappa [T(z_2) - T(z_1)]}{0.74 \left[ \ln \frac{z_2}{z_1} - \Psi_T(\xi_2) + \Psi_T(\xi_1) \right]}, \quad (14)$$

where  $U(z_1)$  and  $U(z_2)$  are the measured velocities at heights  $z_1$  and  $z_2$ , respectively;  $T(z_1)$  and  $T(z_2)$  are the measured temperatures at heights  $z_1$  and  $z_2$ , respectively;  $\xi_1$  and  $\xi_2$  are the stabilities at heights  $z_1$  and  $z_2$ , respectively; and  $\Psi_U$  and  $\Psi_T$  are the correction terms for the velocity and temperature profiles under the condition of stability  $L$ . Under unstable conditions (Stull, 1988), we have the following:

$$\Psi_U(\xi) = \ln \left[ \left( \frac{1+x^2}{2} \right) \left( \frac{1+x}{2} \right)^2 \right] - 2 \arctan(x) + \frac{\pi}{2}, \quad x = (1 - 15\xi)^{1/4}, \quad (15)$$

$$\Psi_T(\xi) = \ln \left[ \left( \frac{1+y}{2} \right)^2 \right], \quad y = (1 - 9\xi)^{1/2}. \quad (16)$$

Under stable conditions (Cheng and Brutsaert, 2005), we have the following:

$$\Psi_U(\xi) = -a \ln \left[ \xi + \left( 1 + \xi^b \right)^{1/b} \right], \quad a = 6.1, \quad b = 2.5, \quad (17)$$

$$\Psi_T(\xi) = -c \ln \left[ \xi + \left( 1 + \xi^d \right)^{1/d} \right], \quad c = 5.3, \quad d = 1.1. \quad (18)$$

Based on Eqs. (13)–(18), the friction velocity  $u_*$  and characteristic temperature  $T_*$  can be determined.

## 3 Measurements and data processing

### 3.1 Introduction of experiments

Observations were collected at two locations (two rectangles in Fig. 1a) from December 2016 to March 2017: a rural site in Gucheng (GC site), Hebei Province and an urban site at the Chinese Academy of Meteorological Sciences (CAMS site) in Beijing. The distance between the two locations is approximately 100 km. According to the theoretical methods

defined in the preceding section, to estimate the aerosol turbulent flux, the ratio of the aerosol mass to the imaginary part of the AERI, the ratio of the temperature to the real part of the AERI, the real and imaginary parts of the atmospheric equivalent refractive index structure parameter (AERISP,  $C_{n,\text{Re}}^2$  and  $C_{n,\text{Im}}^2$ ), the friction speed, and the characteristic temperature must all be obtained. If the free convection condition is satisfied, fewer parameters are required, including the real and imaginary parts of the AERISP, the ratio of the aerosol mass to the imaginary part of the AERI, the ratio of the temperature to the real part of the AERI, and the atmospheric temperature.

Two sets of LASs developed by our research group were installed at the top of the building of the Chinese Academy of Meteorological Sciences (point A in Fig. 1b) and at the top of a two-storey building in the farm of the Central Meteorological Bureau of Gucheng Town, Baoding City (point D in Fig. 1c). The light intensity sampling frequency of the receiving end was 500 Hz, and a file was recorded every 20 min. Then, the real and imaginary parts of the AERISP were calculated.

In the CAMS site, the transmitter end of the LAS was placed on the roof of a building on the east side of the Chinese Academy of Meteorological Sciences, and the receiver end was placed at the top of the Chinese Academy of Meteorological Sciences. The propagation path was along an east–west direction. The distance between the two ends was 550 m as shown in Fig. 1d. The light beam passed over urban buildings, residential areas, and urban roads. The beam height was 43 m. The average height of the building below the beam was 24 m; thus, the zero-displacement was 18 m ( $24 \times 0.67 = 18$ ) (Leclerc and Foken, 2014), and the effective height of the beam was 25 m. At the Beijing observation point, the conventional meteorological parameters are measured on the same roof, 20 m away from the receiving end and in the northwest direction of the receiving end. The measurement heights were 1.5 and 10 m above the roof for air temperature and wind speed. To calculate the aerosol flux, it is necessary to obtain the ratio of the aerosol mass to the imaginary part of AERI and to measure the aerosol mass concentration and visibility. In Haidian District, there is a site to measure the visibility of the near-surface layer (point B in Fig. 1b), and the PM<sub>10</sub> mass concentration measurements were collected at Guanyuan Station (see point C in Fig. 1b). The sampling interval for the visibility and PM<sub>10</sub> mass concentration measurements was 1 h. The measurement height of points B and C in Fig. 1b was approximately 20 m. The ratio of the aerosol mass PM<sub>10</sub> to the imaginary part of the AERI was calculated based on the data. The measurements were collected at the CAMS site from 15 January to 20 March 2017.

In the GC site (point D in Fig. 1c, namely, the LAS position) of Gucheng, Baoding, Hebei, the transmitter of the LAS was placed on the roof of a two-storey building with a



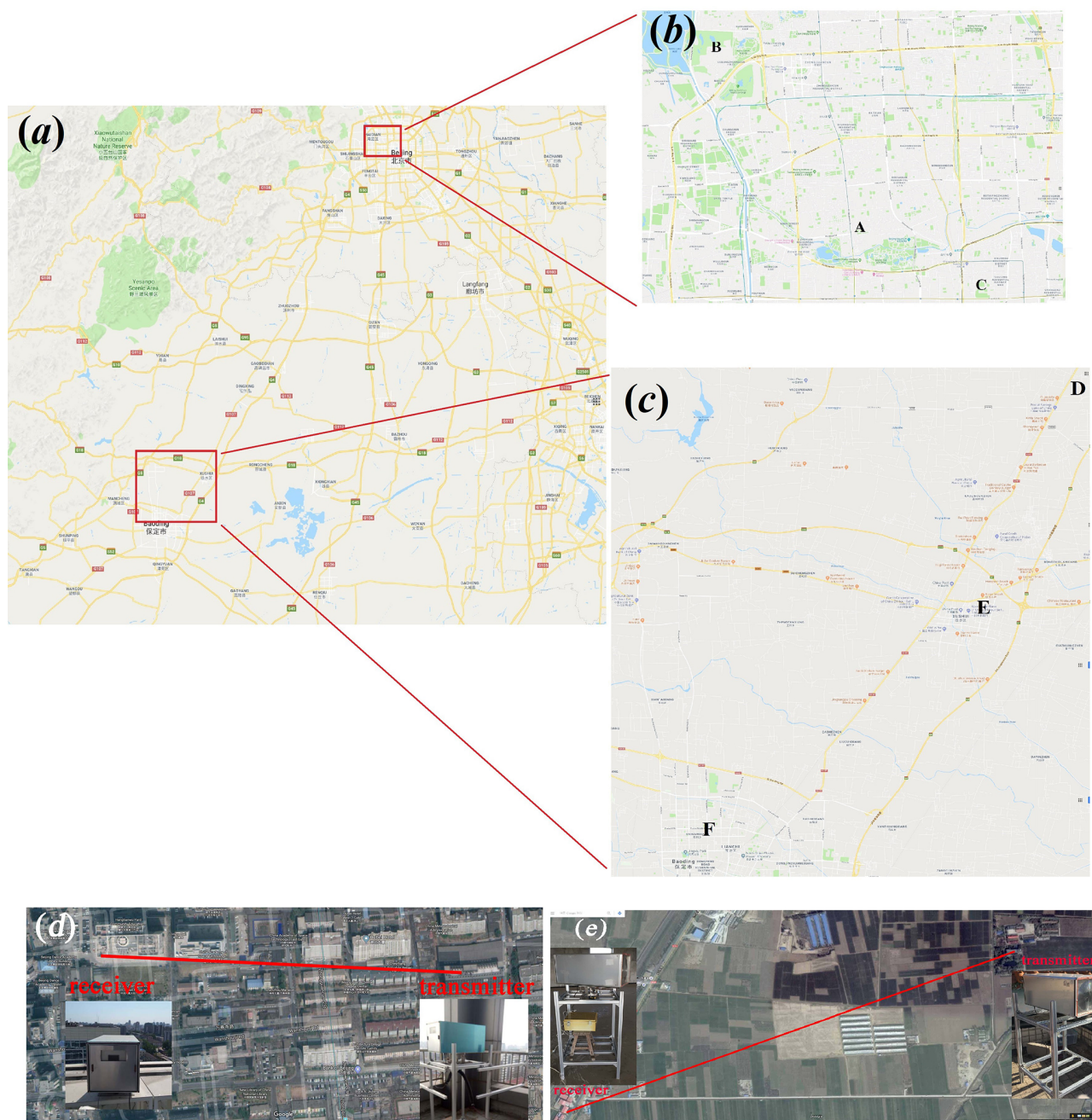


**Figure 1.** Photographs of the measurement site. (a) Map of the experiment area in the Beijing urban area and suburban area and (b) expanded view of the Beijing experiment area, which is marked as the rectangle in (a). (c) Expanded view of the Baoding experiment area, which is marked as the rectangle in (a). (d) Satellite image of the CAMS site and (e) the satellite image of the GC site. Panels (a), (b), (c), and (d) ©Google.

height of 8 m, and the receiving end was located in a room in a three-storey building on the west side of National Highway 107 at the same height as the transmitting end. The distance between the transmitting end and the receiving end was 1670 m. The terrain between the transmitting end and the receiving end was flat, with farmland, a national road, and sporadic trees below the beam, as seen in Fig. 1e. Near the

light beam, there was a 30 m high meteorological observation tower, in which the temperature, relative humidity (RH), and wind speed were measured at five levels (1, 3, 8, 18, and 28 m). The friction speed and characteristic temperature were calculated according to the temperature wind speed profile. Visibility observations were made in Xushui District near the LAS position (see point E in Fig. 1c). The  $\text{PM}_{10}$  mass con-

centration was measured in Beishi District (see point F in Fig. 1c). From Fig. 1c, the three observation points (points D, E and F in Fig. 1c) formed a nearly straight line and were distributed in a northeast–southwest direction. During the experimental observation period, a northeast–southwest wind prevailed; thus, the Xushui District visibility data and Beishi District  $\text{PM}_{10}$  data can approximate the situation of the scintillometer position. The measurements were collected at the GC site from 17 November 2016 to 30 March 2017.

### 3.2 Data quality control

There are two types of variables, namely mean variables and fluctuation variables. Mean variables include temperature, wind speed, wind direction,  $\text{PM}_{10}$ , and visibility for averages of 30 min or 60 min. Data quality control for the mean variables was conducted by comparing the measured data at different heights or at different stations. Variables between different heights and different locations that have the same trend are considered high quality. All the measured mean data were determined to be adequate. Fluctuation variables include the high-frequency intensity fluctuation data measured by the LAS, the real and imaginary parts of the AERISP, and the calculated aerosol flux. Quality control mainly consists of the elimination of spikes and supplementing missing data.

Peaks in the light intensity fluctuation data appear because the received signal quickly increases when the light signal is blocked, such as due to birds along the transmission path. The data processing program automatically determines this situation. When this happens, the current 20 min period is rejected. For the real and imaginary parts of the AERISP and the aerosol flux data, (a) 3 times the standard deviation (SD) of the anomaly and (b) 3 times the SD of the difference between adjacent moments (AMD) were determined. A trend of 2 h averages, namely, 6-point moving averages, was first obtained. Then, the difference between the measured value and the trend at each moment was calculated, and the mean and SD of the difference were also calculated. The data with differences from the trend exceeding 3 times the SD were considered as spikes. The method for judging 3 times the SD of the AMD was first to calculate the AMD and then to calculate the mean and SD of the AMDs. Any data whose AMD deviated from the mean of the AMD by more than 3 times the SD of the AMD were considered an error. Less than 5 % of the data were found to contain spikes or errors.

The data determined to be errors were supplemented with the average of the nearby observations. Of course, if data were missing over a long period, the missing gap could not be filled. For this situation, further gap-filling was not considered.

Other errors exist in the measurements using a LAS due to specific reasons (Moene et al., 2009); for example, the impact of the deviation of the shape of spectrum from von Karman's scheme and the intermittent variations in the characteristics

of that spectrum on the LAS signal were not considered in this study.

## 4 Results

First, the visibility and  $\text{PM}_{10}$  aerosol mass concentration results at the CAMS site and the GC site are given and compared. Then, the characteristics of aerosol transport in typical weather conditions at the CAMS site and the GC site are discussed. Finally, the aerosol flux characteristics during the HPEs are analysed.

### 4.1 Relationship between $n_{\text{im}}$ and $\text{PM}_{10}$

To obtain the ratio of the atmospheric aerosol mass concentration to the imaginary part of the AERI ( $n_{\text{im}}$ )  $R_{\text{MN}}$ ,  $\text{PM}_{10}$ , and visibility were measured.

The maximum  $\text{PM}_{10}$  concentration in the Baoding area appeared at 01:00 local time (LT) on 28 January 2017 (up to  $1071 \mu\text{g m}^{-3}$ ), and the maximum  $\text{PM}_{10}$  concentration in the Beijing area appeared at 02:00 LT on 28 January 2017 (up to  $917 \mu\text{g m}^{-3}$ ). This heavy pollution event swept through Beijing and the surrounding areas, reaching a maximum at almost the same time. The visibility at the corresponding time was less than 500 m. The imaginary part of the AERI can be calculated from the visibility according to Eq. (7). Figure 2a shows a relationship plot of the imaginary parts of the AERI and  $\text{PM}_{10}$  data measured in the Beijing area; there is a strong correlation between the AERI and aerosol particle mass concentration, with a linear correlation coefficient of 0.96. The fitted line in Fig. 2a has a slope of  $3845 \text{ kg m}^{-3}$ . Therefore,  $R_{\text{MN}}$  was taken as  $3845 \text{ kg m}^{-3}$  for the Beijing area to estimate the aerosol vertical turbulent flux. Similarly, Fig. 2b shows the results for the Baoding area, and  $R_{\text{MN}}$  was set to  $3711 \text{ kg m}^{-3}$  for the Baoding area to estimate the aerosol vertical turbulent flux. The two ratio coefficients are relatively close. Figure 2a and b also show that in the case of light pollution, Beijing's  $R_{\text{MN}}$  is slightly larger.

Furthermore, Fig. 2a and b show that although there is a significant scattering between  $\text{PM}_{10}$  and  $n_{\text{IM}}$  that may be attributed to a significant separation between the two measurement locations for visibility and  $\text{PM}_{10}$ , there is a strong linear correlation between the imaginary part of the AERI and  $\text{PM}_{10}$ . The imaginary part of the AERI has a slightly stronger relationship with the  $\text{PM}_{10}$  data obtained in the Baoding area than in the Beijing area.

$R_{\text{MN}}$  should be obtained by simultaneously measuring  $M_a$  and the imaginary part of the AERI at the same location with the LAS, so that real-time  $R_{\text{MN}}$  can be obtained. For the GC site and CAMS site, measuring positions of  $\text{PM}_{10}$  and visibility are a little far from LAS measurement. So a constant ratio  $R_{\text{MN}}$  is more representative than a simultaneous value.



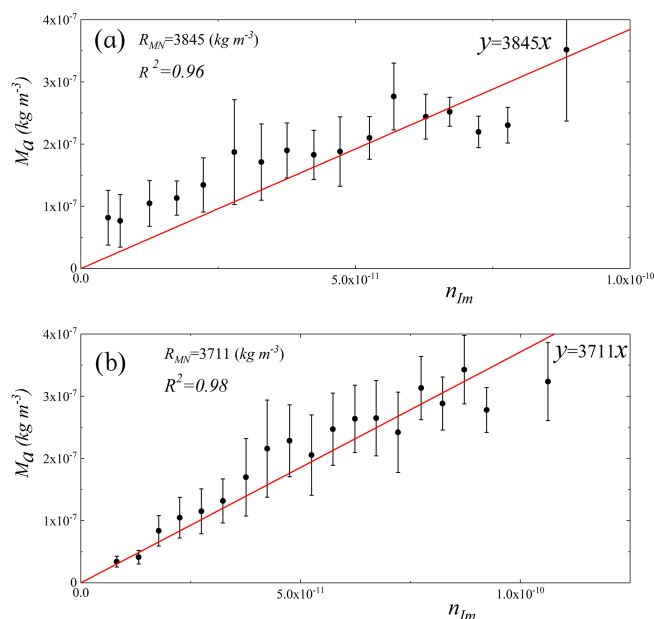


**Figure 2.** Relationship plot of aerosol mass concentration  $M_a$  and the imaginary part of the AERI for (a) the Beijing area and (b) the Baoding area.

The following provides the results of the aerosol turbulent flux under typical weather conditions in Beijing and Baoding for the period from 10 to 17 March 2017.

#### 4.2 Characteristics of aerosol flux in the Beijing region

To analyse the aerosol turbulent flux characteristics, we present the time series of the conventional meteorological parameters. The time series of temperature, RH, wind speed, wind direction,  $PM_{10}$ ,  $C_{n,Re}^2$ ,  $C_{n,Im}^2$ , and aerosol flux are shown in Fig. 3a–h, respectively. The temperature has a distinct diurnal variation, indicating that this period had primarily sunny weather. The RH from 10 to 17 March 2017, was less than 60 %, and the RH for most of the period was less than 30 %. The wind speed was low; only during the period from 11 to 14 March was the wind moderately strong. At 06:00 LT on 12 March, the maximum wind speed was  $4.2 \text{ m s}^{-1}$ . At that time, the wind direction has diurnal variation, which is related to the sea–land breeze, valley wind, and urban heat island circulation which may exist under the control of weak weather system (Li et al., 2019). Moreover, two light pollution events occurred (MEP, 2012) on 11 and 16 March, with  $PM_{10}$  concentrations approaching  $200 \mu\text{g m}^{-3}$ . From the data of  $C_{n,Re}^2$  and  $C_{n,Im}^2$  in Fig. 3f and g, the real part of the AERISP  $C_{n,Re}^2$  has obvious diurnal variations, i.e. smaller in the morning and at night and larger at noon. The imaginary part of the AERISP  $C_{n,Im}^2$  had no distinct diurnal variation. According to Fig. 3g, there are some peak values, i.e. some sudden increases and decreases, which

may be related to sudden changes in wind direction, as shown in Fig. 3d.

The LAS at the CAMS site was located in the roughness layer, so the local similarity theory should in principle be applied to flux calculation. Because there was no measurement of wind speed and temperature profiles near the LAS measurement location, the friction velocity and characteristic temperature could not be calculated. We (Yuan et al, 2015) conducted a test experiment for aerosol vertical flux in Hefei, China, using free convection assumptions and local similarity theories to calculate aerosol fluxes. Comparison of the calculation results of the two methods shows that very unstable conditions account for about 62 % of the time, and the relative difference is about 5 %. Under weak unstable and stable conditions, the relative error is about 15 %.

From the aerosol flux time series given in Fig. 3h, the aerosol flux is large at noon and small in the morning and at night, which is mainly because of the strong convection at noon. However, large aerosol fluxes also occurred on the nights of 11 and 12 March, which were related to high wind speeds. The mean aerosol flux measured at this observation point during this period was  $0.0039 \text{ mg m}^{-2} \text{ s}^{-1}$ .

#### 4.3 Characteristics of aerosol flux at the GC site

Similarly, Fig. 4a–d provide the time series of temperature, RH, wind speed, and wind direction at 3 and 18 m for the GC site, and Fig. 4e–h show the  $PM_{10}$ ,  $C_{n,Re}^2$ ,  $C_{n,Im}^2$ , and aerosol flux curves over time. According to Fig. 4a, the temperatures at both heights show distinct diurnal variations. The daytime is characterized by unstable stratification, and at night, stable stratification prevails. Moreover, in the morning and evening, there is a transition period between stable and unstable stratification. Here,  $u_*$ ,  $T_*$ , and MO length  $L$  were calculated from the wind speed and temperature measured at 3 and 18 m on a meteorological tower. Figure 4b shows a plot of the two levels of RH over time, again with apparent diurnal variations. The RH of the GC site was lower at the CAMS site. Figure 4c and d provide the time series of wind speeds and wind directions at two levels. At 06:00 on 12 March, the wind speed was relatively high, and the maximum at 18 m was  $6.5 \text{ m s}^{-1}$ . At the same time, the maximum wind speed was reached in the Beijing area, although the speed was lower in Beijing. The overall trend of wind direction at the GC site was more consistent with the results of the CAMS site.

Figure 4e shows the  $PM_{10}$  trend of over time. There were two light pollution events on 11 and 16 March. The overall trend is the same as in Fig. 3e. Figure 4f and g show the time series of the imaginary and real parts of the AERISP for the GC site. The real part of the AERISP is large at noon, and the optical turbulence is strong. The real part of the AERISP is small during the morning and evening, and the corresponding turbulence is weak. The imaginary part of the AERISP given in Fig. 4g does not show an apparent diurnal variation, and there may be some sharp peaks.

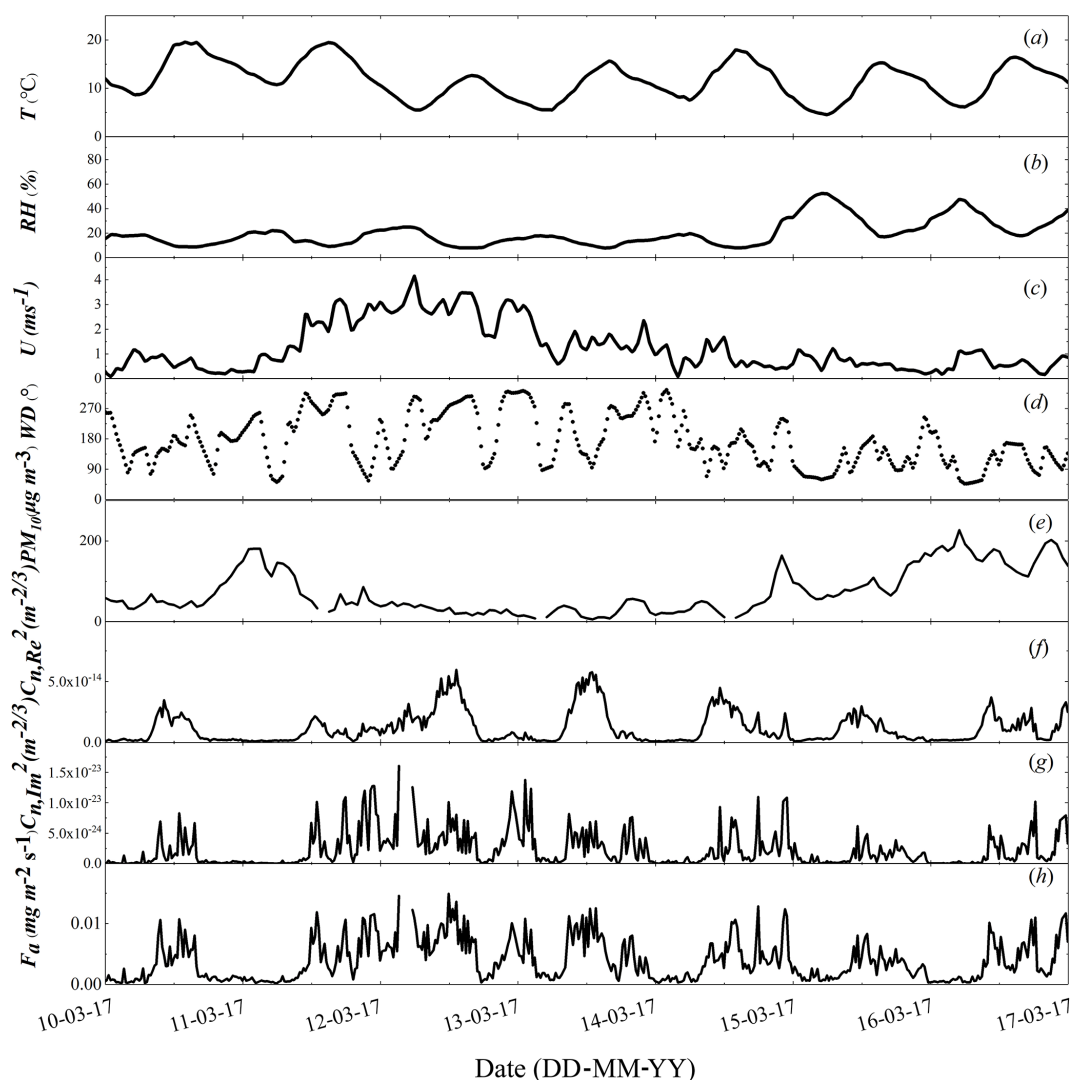


**Figure 3.** Temporal variations in (a) air temperature, (b) RH, (c) wind speed, (d) wind direction, (e)  $\text{PM}_{10}$ , (f) real part of the AERISP, (g) imaginary part of the AERISP, and (h) aerosol mass flux in the Beijing area from 10 to 17 March 2017.

Figure 4h shows the aerosol mass vertical flux changes over time. The aerosol flux has a significant diurnal variation characteristic associated with turbulent transport near the surface. The mean aerosol flux measured at the GC site during this period was  $0.0016 \text{ mg m}^{-2} \text{ s}^{-1}$ . This value is much smaller than the results for the CAMS site. Human activities contribute to increased water vapour releases in urban areas compared to rural areas, as observed by Dou et al. (2014), and especially for the night-time SBL in winter. During our observation period, the RH of the city was lower than the rural area. However, human activities cause more aerosol particles in urban areas than in rural areas.

#### 4.4 Aerosol flux during HPEs

In the winter of 2016, there were several HPEs. A heavy pollution event began on 1 December 2016 and ended on

10 January 2017. Relevant observational experiments were performed in the Beijing and Baoding areas, including observations of meteorological parameters and aerosol parameters, to understand the causes of the heavy pollution.

According to the definition of HPEs and classification, there were seven TS stages in the 2016 winter heavy pollution event, and the AS stage appeared immediately after four TS stages. These included 00:00 LT on 1 December to 03:20 LT on 4 December, 18:40 LT on 15 December to 00:00 LT on 22 December, 00:00 LT on 29 December to 2 January, and 00:00 LT and 08:40 LT on 2 January to 00:00 LT on 5 January.

During this period, we used a LAS to conduct an observational study of the vertical aerosol flux in the GC site, which was from 00:00 LT on 1 December, 2016, to 00:00 LT on 22 December 2016. No corresponding observations were

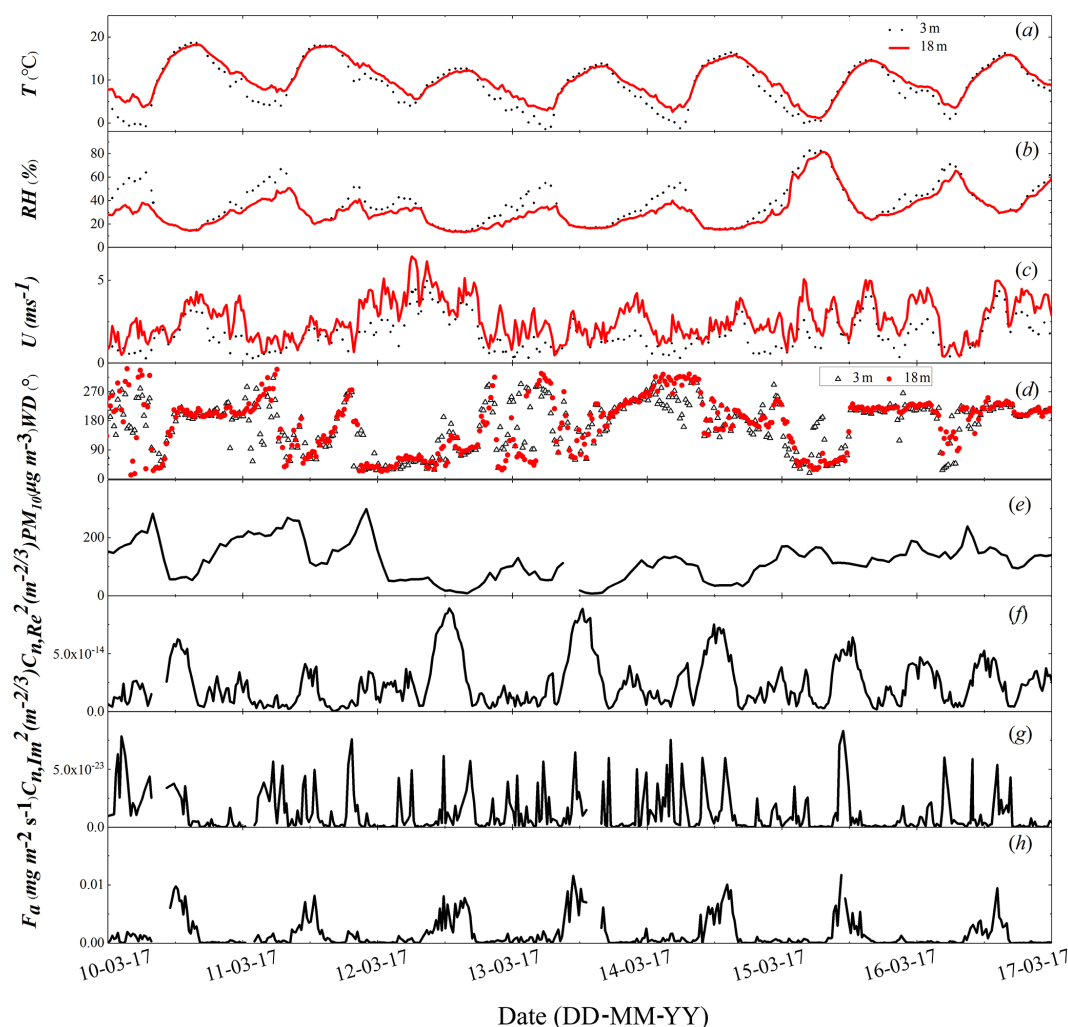


**Figure 4.** Temporal variations in (a) air temperature, (b) RH, (c) wind speed, (d) wind direction, (e)  $\text{PM}_{10}$ , (f) real part of the AERISP, (g) imaginary part of the AERISP, and (h) aerosol mass flux in the Baoding area from 10 to 17 March 2017.

made at the Beijing site during this period. Here, we first discuss the observation results of the GC site, Baoding City, as shown in Fig. 5. Figure 5a shows the time series of the aerosol vertical turbulent flux. Figure 5b–g indicate the time series for the real and imaginary parts of the AERISP, the temperature and RH at 18 m, and the wind speed and direction. Purple curves indicate the TS stages, red curves show the AS stages, and grey curves show the RS stages.

According to Fig. 5a, in the TS stages and the RS stages, the aerosol flux exhibited diurnal variations, while the AS stage did not show a diurnal variation. There were some peaks in the TS stage. The average aerosol flux of the TS stages was  $0.00065 \text{ mg m}^{-2} \text{ s}^{-1}$ , the average value of the AS stages was  $0.00025 \text{ mg m}^{-2} \text{ s}^{-1}$ , and the average value of the RS stages was  $0.00063 \text{ mg m}^{-2} \text{ s}^{-1}$ . The aerosol turbulent fluxes in the TS and RS stages were similar, while the aerosol turbulent flux in the AS stage was much smaller than the TS and RS stages.

According to Fig. 5b–c, the imaginary structure parameters and the real structure parameters of the refractive index in the TS and RS stages exhibited diurnal variations, while the AS stage did not exhibit a diurnal variation. Figure 5d shows that except for the second AS event (22:00 LT on 19 December to 00:00 LT ON 22 December 2016), the temperature showed a diurnal variation. During the AS stage, the RH (see Fig. 5e) was close to 100 %, while the RH during the TS and RS stages was lower. Moreover, Fig. 5f shows that during this time, the wind speed was relatively weak, although the wind speed was slightly stronger on 5 December. As shown in Fig. 5g, during the TS and AS stages, southerly winds prevailed, while during the RS period, northerly winds prevailed. The high wind speed and convection in the TS and RS stages contributed to the upward transport of aerosol particles, whereas the low wind speed and stable stratification in the AS stage were not conducive to the upward transport of aerosol particles.

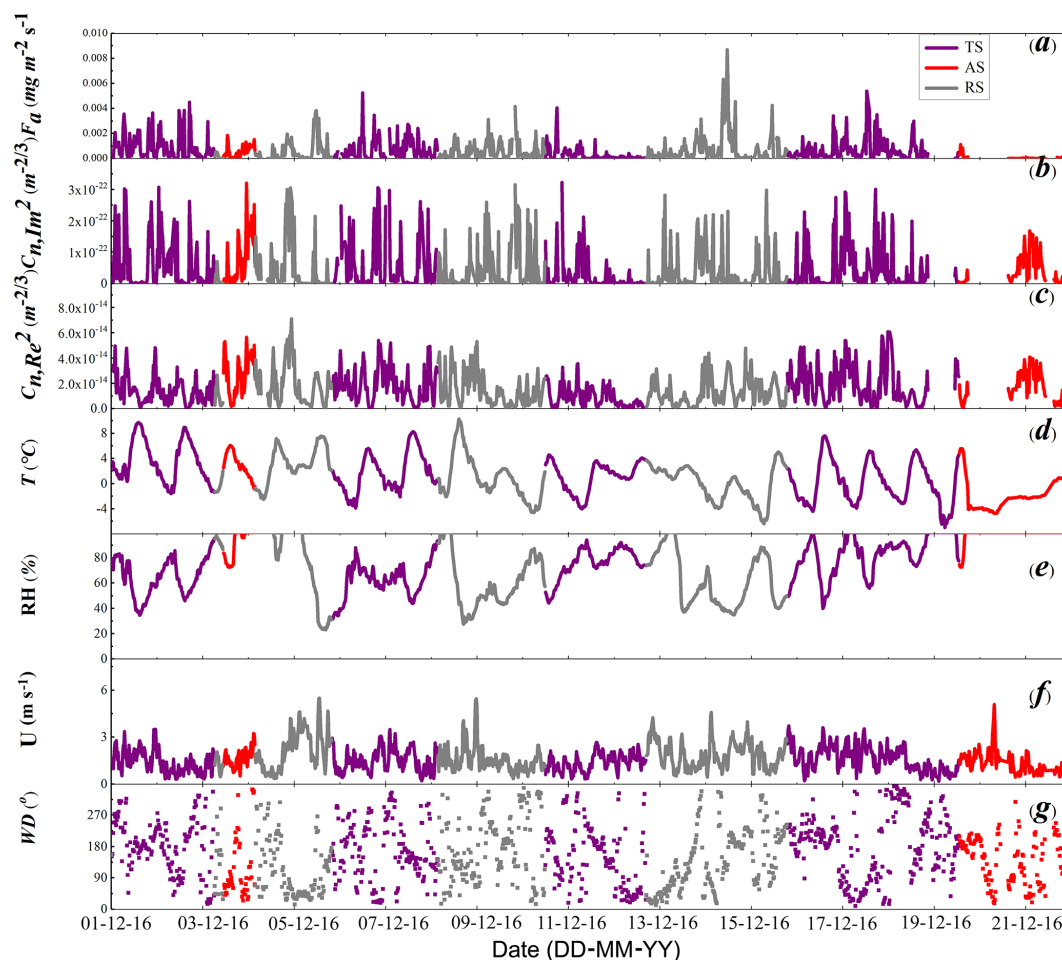


**Figure 5.** Temporal variations in (a) aerosol flux, (b) imaginary part of the AERISP, (c) real part of the AERISP (d) air temperature, (e) RH, (f) wind speed, and (g) wind direction in the Baoding area during a heavy pollution period, i.e. 1 to 22 December 2016.

During the heavy pollution period from 1 December 2016 to 10 January 2017, we did not conduct surface aerosol flux observations at the CAMS site. From 25 to 31 January, the pollution in the Beijing area also reached the level of heavy pollution. During this HPE, a measurement of surface aerosol fluxes at the CAMS site was conducted. Figure 6 shows the results of the meteorological and pollutant observations for six days from 00:00 LT on 25 to 00:00 LT on 31 January 2017. According to Fig. 6, northerly winds prevailed after noon on January 26, when the concentration of  $\text{PM}_{10}$  dropped rapidly from  $254 \mu\text{g m}^{-3}$  at 12:00 LT to  $5 \mu\text{g m}^{-3}$  at 15:00 LT. During the period 12:00–00:00 LT on 26 January, the average wind speed was  $2.6 \text{ m s}^{-1}$ . On 27 January, southerly winds prevailed, the average wind speed was only  $0.8 \text{ m s}^{-1}$ , and the aerosol concentration ( $\text{PM}_{10}$ ) increased slowly; the increase began at 06:30 LT before growing rapidly at 17:50 LT, reaching more than  $300 \mu\text{g m}^{-3}$  at 23:00 and  $917 \mu\text{g m}^{-3}$  at 02:00 LT on 28 January, which was the maximum aerosol concentration over the 6 d period. Then, the aerosol concentration decreased gradually. The av-

erage wind speed on 27 January was  $0.6 \text{ m s}^{-1}$ , southerly winds prevailed, and the mean  $\text{PM}_{10}$  concentration was  $440 \mu\text{g m}^{-3}$ , which constitutes a severe pollution level. The average  $\text{PM}_{10}$  concentration during the period from 00:00 LT on 25 January to 00:00 LT on 31 January was  $170 \mu\text{g m}^{-3}$ .

According to the previous characteristics for the TS and AS stages, a period of southerly winds can be determined as the TS stage. Thus, 27 January can be designated as the TS stage, 28 January can be determined as the AS stage, and 29 January can be determined as the RS stage. During Beijing's heavy pollution event in January 2017 (25 to 31 January 2017), the mean aerosol vertical flux in the TS stage was  $0.0024 \text{ mg m}^{-2} \text{s}^{-1}$ , the average value during the AS stage was  $0.00087 \text{ mg m}^{-2} \text{s}^{-1}$ , and the RS stage was  $0.0049 \text{ mg m}^{-2} \text{s}^{-1}$ . The overall average value was  $0.0032 \text{ mg m}^{-2} \text{s}^{-1}$ .

Even during heavy pollution events, the RH in Beijing was lower than in the outer suburbs. According to Fig. 6e, the RH exceeded 60 % in the period from 03:00 LT to 06:00 LT on 26 January, where the maximum value was 63 %, and the RH

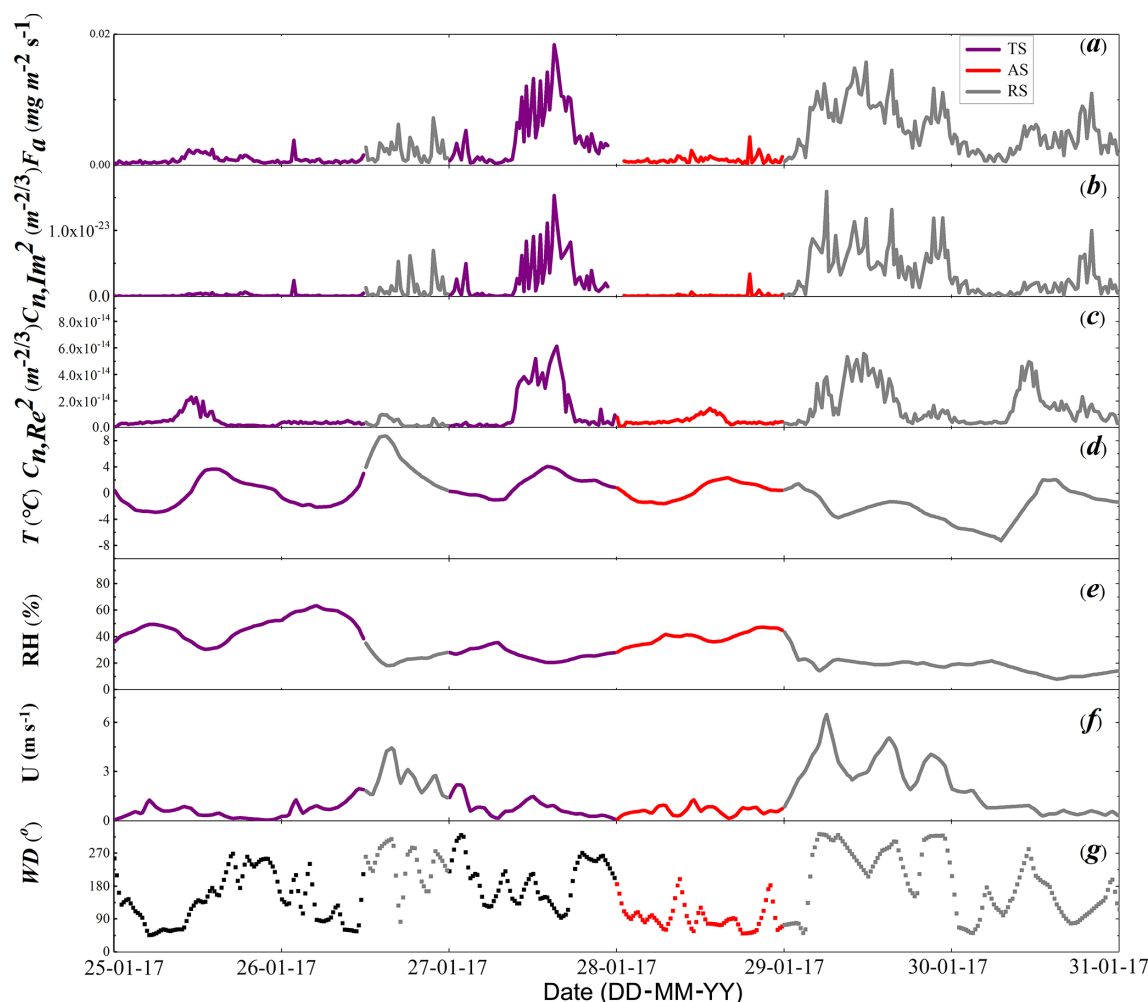


**Figure 6.** Temporal variations in (a) aerosol flux, (b) imaginary part of the AERISP, (c) real part of the AERISP (d) air temperature, (e) RH, (f) wind speed, and (g) wind direction in the Beijing area during a heavy pollution period, i.e. 25 to 31 January 2017.

was less than 60 % in the remaining periods. In urban areas, when the RH is low, heavy pollution incidents can occur. In Beijing, during the AS stage, the vertical flux of aerosol was less than during the TS and RS stages.

## 5 Discussions and conclusions

During the winter of 2016 and the spring of 2017, HPEs frequently occurred in the BTH area.

This study investigated the aerosol vertical mass flux and compared its magnitude during different stages of HPEs, including RSs, TSs, and ASs, in two representative urban and rural sites, including the CAMS site in Beijing and the GC site in Hebei Province. Based on the light propagation theory and surface-layer similarity theory, the aerosol vertical mass flux was obtained by combining LAS observations, surface  $\text{PM}_{2.5}$  and  $\text{PM}_{10}$  mass concentrations, and meteorological observations, including air temperature and RH.

We found that under favourable meteorological conditions for pollution dispersion, i.e. from 10 to 17 March 2017, the vertical aerosol mass flux exhibited striking diurnal variations, with the mass fluxes reaching peak values at noon and lowering in the morning and evening. During the HPEs from 25 to 31 January 2017 in Beijing, the vertical aerosol mass flux varied substantially during the different stages. Specifically, the mean mass flux decreased by 51 % from  $0.0049 \text{ mg m}^{-2} \text{ s}^{-1}$  in the RSs to  $0.0024 \text{ mg m}^{-2} \text{ s}^{-1}$  in the TSs, which was partly due to the wind speed reduction from strong northerly winds in the RSs to southerly winds in the TSs. During the ASs, the mean mass flux decreased further to  $0.00087 \text{ mg m}^{-2} \text{ s}^{-1}$ , which accounted for approximately one-third of the flux during the TSs. The weakened mass flux would further facilitate aerosol accumulation. During the HPE from 1 to 22 December 2016, in Gucheng, the mean mass flux was similar in the RSs and TSs, ranging from  $0.00063$  to  $0.00065 \text{ mg m}^{-2} \text{ s}^{-1}$ . This is partly because Gucheng was less affected by strong northerly winds than



Beijing. Thus, the wind speed varied slightly from the RSs to TSs. However, the mass flux decreased substantially to  $0.00025 \text{ mg m}^{-2} \text{ s}^{-1}$  in the ASs, which was merely one-third of the mean flux in the TSs.

Based on our measurement results, it can be seen that from the TS to the AS, the aerosol vertical turbulent flux decreased, but the aerosol particle concentration with surface layer increased. It is inferred that in addition to the contribution of regional transport from upwind areas during the TS, suppression of vertical turbulence mixing confining aerosols to a shallow boundary layer increased accumulation.

In this study, the aerosol emission flux was also estimated in these two rural and urban sites. Generally, compared with the emissions in spring, we found that in winter, the near-ground emissions were weaker in suburban areas and were similar in urban areas. In suburban areas, although the aerosol concentrations were relatively high (Shen et al., 2018), the upward emitted aerosol flux was smaller than in urban areas. During the ASs of the HPEs, the aerosol emission flux from near-ground emission sources was weaker than for the RSs and TSs at both the CAMS and GC sites, which indicates that surface pollutant emissions are not the major cause of explosive  $\text{PM}_{2.5}$  growth. During the ASs with weak solar radiation, the factors most associated with aerosol concentration changes were horizontal transport and BL height variations, which might be the leading causes of increased  $\text{PM}_{2.5}$ . This is in line with previous studies that the main reason for the explosive growth of aerosol concentration during AS is attributed to the horizontal transport during TS. The TS will definitely appear before AS. The south or southwest wind will always appear in the TS, and the concentration of  $\text{PM}_{10}$  in Baoding is higher than the mass of  $\text{PM}_{10}$  in Beijing, which is generally maintained for one to two days. Except for the southerly or southwesterly winds for one to two days, there will be no AS in Beijing. Even if it is a southerly or southwesterly wind, if the wind speed is too small ( $< 1 \text{ m s}^{-1}$ ), AS will not appear. Only the southerly or southwesterly wind with a wind speed greater than a specific value ( $> 1.5 \text{ m s}^{-1}$ ), and the concentration of  $\text{PM}_{10}$  in the area to the south of Beijing is higher than that in Beijing, and then there will be AS after a small wind (Zhong et al., 2018b, c; Zhang et al., 2018).

Compared to the results (Yuan et al., 2016) from Hefei, China, a small to medium-sized provincial capital city in East China, the measured aerosol mass fluxes in Beijing are almost at the same amount. A series of measures and actions have been made for emission reduction in Beijing, and the main emission is from vehicles. The difference in aerosol mass flux may be small.

Due to the lack of necessary experimental conditions, such as meteorological towers and EC systems, current experimental results cannot be compared with EC methods. According to the literature data, the two methods have been compared indirectly, and the estimated aerosol flux under different measurement conditions is consistent in magnitude

(Yuan et al., 2016). However, a direct comparison of the two methods is in development.

Compared with the EC method, the aerosol flux has high spatial representativeness based on the principle of light propagation, and there is no need to install a tall tower. However, the estimation of aerosol fluxes using the LAS method still has theoretical and practical deficiencies. At present, the LAS method for the aerosol flux regards the aerosol particles as ordinary scalar molecules. At the same time, based on the assumption of the equivalent medium, the imaginary part of the AERI is presumed to be proportional to the aerosol mass concentration. This is often not the case. The actual turbulence spectrum shape may deviate from the von Karman spectrum, and turbulence intermittent and scintillation saturation can also occur (Moene et al., 2009). The applicability of the near-surface layer similarity theory to the aerosol particle motion under stable layer conditions also has many problems. The formation of new particles and changes in aerosol particle size distribution also affect the scintillation in light propagation. There are also practical problems such as untimely maintenance, rainfall and low visibility, and platform vibrations required for observation. All these problems will cause errors in final estimates, so more theoretical and experimental research is needed.

**Data availability.** Requests for data that support the findings of this study can be sent to [rmyuan@ustc.edu.cn](mailto:rmyuan@ustc.edu.cn).

**Author contributions.** RY and XZ designed experiments and wrote the paper. RY, HL, YG, BS, YW, JZ, and XT carried out experiments. RY analysed experimental results. YL and ZG designed experiments and discussed the results.

**Competing interests.** The authors declare that they have no conflict of interest.

**Acknowledgements.** We also thank two anonymous reviewers for their constructive and helpful comments.

**Financial support.** This research has been supported by the National Key Research and Development Program (grant no. 2016YFC0203306), and the National Natural Science Foundation of China (grant nos. 41775014 and 51677175).

**Review statement.** This paper was edited by Tuukka Petäjä and reviewed by two anonymous referees.



## References

- Ahlm, L., Krejci, R., Nilsson, E. D., Martensson, E. M., Vogt, M., and Artaxo, P.: Emission and dry deposition of accumulation mode particles in the Amazon Basin, *Atmos. Chem. Phys.*, 10, 10237–10253, <https://doi.org/10.5194/acp-10-10237-2010>, 2010a.
- Ahlm, L., Nilsson, E. D., Krejci, R., Martensson, E. M., Vogt, M., and Artaxo, P.: A comparison of dry and wet season aerosol number fluxes over the Amazon rain forest, *Atmos. Chem. Phys.*, 10, 3063–3079, <https://doi.org/10.5194/acp-10-3063-2010>, 2010b.
- Akagi, S. K., Yokelson, R. J., Wiedinmyer, C., Alvarado, M. J., Reid, J. S., Karl, T., Crounse, J. D., and Wennberg, P. O.: Emission factors for open and domestic biomass burning for use in atmospheric models, *Atmos. Chem. Phys.*, 11, 4039–4072, <https://doi.org/10.5194/acp-11-4039-2011>, 2011.
- Bond, T. C., Streets, D. G., Yarber, K. F., Nelson, S. M., Woo, J. H., and Klimont, Z.: A technology-based global inventory of black and organic carbon emissions from combustion, *J. Geophys. Res.-Atmos.*, 109, D14203, <https://doi.org/10.1029/2003jd003697>, 2004.
- Brion, J., Chakir, A., Charbonnier, J., Daumont, D., Parisse, C., and Malicet, J.: Absorption spectra measurements for the ozone molecule in the 350–830 nm region, *J. Atmos. Chem.*, 30, 291–299, <https://doi.org/10.1023/a:1006036924364>, 1998.
- Brooks, I. M., Yelland, M. J., Upstill-Goddard, R. C., Nightingale, P. D., Archer, S., d'Asaro, E., Beale, R., Beatty, C., Blomquist, B., Bloom, A. A., Brooks, B. J., Cluderay, J., Coles, D., Dacey, J., DeGrandpre, M., Dixon, J., Drennan, W. M., Gabriele, J., Goldson, L., Hardman-Mountford, N., Hill, M. K., Horn, M., Hsueh, P.-C., Huebert, B., de Leeuw, G., Leighton, T. G., Liddicoat, M., Lingard, J. J. N., McNeil, C., McQuaid, J. B., Moat, B. I., Moore, G., Neill, C., Norris, S. J., O'Doherty, S., Pascal, R. W., Prytherch, J., Rebozo, M., Sahlee, E., Salter, M., Schuster, U., Skjelvan, I., Slagter, H., Smith, M. H., Smith, P. D., Srokosz, M., Stephens, J. A., Taylor, P. K., Telszewski, M., Walsh, R., Ward, B., Woolf, D. K., Young, D., and Zemelink, H.: Physical exchanges at the air-sea interface uk-solas field measurements, *B. Am. Meteorol. Soc.*, 90, 629–644, <https://doi.org/10.1175/2008bams2578.1>, 2009.
- Buzorius, G., Rannik, U., Makela, J. M., Vesala, T., and Kulmala, M.: Vertical aerosol particle fluxes measured by eddy covariance technique using condensational particle counter, *J. Aerosol Sci.*, 29, 157–171, [https://doi.org/10.1016/s0021-8502\(97\)00458-8](https://doi.org/10.1016/s0021-8502(97)00458-8), 1998.
- Cao, J., Xu, H., Xu, Q., Chen, B., and Kan, H.: Fine Particulate Matter Constituents and Cardiopulmonary Mortality in a Heavily Polluted Chinese City, *Environ. Health Persp.*, 120, 373–378, <https://doi.org/10.1289/ehp.1103671>, 2012.
- Ceburnis, D., Rinaldi, M., Ovadnevaite, J., Martucci, G., Giulianelli, L., and O'Dowd, C. D.: Marine submicron aerosol gradients, sources and sinks, *Atmos. Chem. Phys.*, 16, 12425–12439, <https://doi.org/10.5194/acp-16-12425-2016>, 2016.
- Chen, Y., Tian, C., Feng, Y., Zhi, G., Li, J., and Zhang, G.: Measurements of emission factors of PM<sub>2.5</sub>, OC, EC, and BC for household stoves of coal combustion in China, *Atmos. Environ.*, 109, 190–196, <https://doi.org/10.1016/j.atmosenv.2015.03.023>, 2015.
- Cheng, Y. G. and Brutsaert, W.: Flux-profile relationships for wind speed and temperature in the stable atmospheric boundary layer, *Bound.-Lay. Meteorol.*, 114, 519–538, <https://doi.org/10.1007/s10546-004-1425-4>, 2005.
- DeBruin, H. A. R., vandenHurk, B., and Kohsiek, W.: The scintillation method tested over a dry vineyard area, *Bound.-Lay. Meteorol.*, 76, 25–40, 1995.
- Dou, J., Wang, Y., and Miao, S.: Fine Spatial and Temporal Characteristics of Humidity and Wind in Beijing Urban Area, *J. Appl. Meteorol. Sci.*, 25, 559–569, 2014.
- Dubovik, O., Holben, B., Eck, T. F., Smirnov, A., Kaufman, Y. J., King, M. D., Tanre, D., and Slutsker, I.: Variability of absorption and optical properties of key aerosol types observed in worldwide locations, *J. Atmos. Sci.*, 59, 590–608, 2002.
- Elbert, W., Taylor, P. E., Andreae, M. O., and Poeschl, U.: Contribution of fungi to primary biogenic aerosols in the atmosphere: wet and dry discharged spores, carbohydrates, and inorganic ions, *Atmos. Chem. Phys.*, 7, 4569–4588, <https://doi.org/10.5194/acp-7-4569-2007>, 2007.
- EPD, E. P. D.: Technical regulation on ambient air quality index (on trial), Beijing, 12 pp., 2012.
- Evans, J. G. and De Bruin, H. A. R.: The Effective Height of a Two-Wavelength Scintillometer System, *Bound.-Lay. Meteorol.*, 141, 165–177, <https://doi.org/10.1007/s10546-011-9634-0>, 2011.
- Farmer, D. K., Kimmel, J. R., Phillips, G., Docherty, K. S., Worsnop, D. R., Sueper, D., Nemitz, E., and Jimenez, J. L.: Eddy covariance measurements with high-resolution time-of-flight aerosol mass spectrometry: a new approach to chemically resolved aerosol fluxes, *Atmos. Meas. Tech.*, 4, 1275–1289, <https://doi.org/10.5194/amt-4-1275-2011>, 2011.
- Gordon, M., Staebler, R. M., Liggio, J., Vlasenko, A., Li, S.-M., and Hayden, K.: Aerosol flux measurements above a mixed forest at Borden, Ontario, *Atmos. Chem. Phys.*, 11, 6773–6786, <https://doi.org/10.5194/acp-11-6773-2011>, 2011.
- Graham, B., Guyon, P., Taylor, P. E., Artaxo, P., Maenhaut, W., Glovsky, M. M., Flagan, R. C., and Andreae, M. O.: Organic compounds present in the natural Amazonian aerosol: Characterization by gas chromatography-mass spectrometry, *J. Geophys. Res.-Atmos.*, 108, D24, <https://doi.org/10.1029/2003jd003990>, 2003.
- Guo, H., Xu, M., and Hu, Q.: Changes in near-surface wind speed in China: 1969–2005, *Int. J. Climatol.*, 31, 349–358, <https://doi.org/10.1002/joc.2091>, 2011.
- Guo, S., Hu, M., Zamora, M. L., Peng, J. F., Shang, D. J., Zheng, J., Du, Z. F., Wu, Z., Shao, M., Zeng, L. M., Molina, M. J., and Zhang, R. Y.: Elucidating severe urban haze formation in China, *P. Natl. Acad. Sci. USA*, 111, 17373–17378, <https://doi.org/10.1073/pnas.1419604111>, 2014.
- Harrison, R. M., Dall'Osto, M., Beddows, D. C. S., Thorpe, A. J., Bloss, W. J., Allan, J. D., Coe, H., Dorsey, J. R., Gallagher, M., Martin, C., Whitehead, J., Williams, P. I., Jones, R. L., Langridge, J. M., Benton, A. K., Ball, S. M., Langford, B., Hewitt, C. N., Davison, B., Martin, D., Petersson, K. F., Henshaw, S. J., White, I. R., Shallcross, D. E., Barlow, J. F., Dunbar, T., Davies, F., Nemitz, E., Phillips, G. J., Helfter, C., Di Marco, C. F., and Smith, S.: Atmospheric chemistry and physics in the atmosphere of a developed megacity (London): an overview of the REPARTEE experiment and its conclusions, *Atmos. Chem. Phys.*, 12, 3065–3114, <https://doi.org/10.5194/acp-12-3065-2012>, 2012, 2012.

- Hartogensis, O. K., Watts, C. J., Rodriguez, J. C., and De Bruin, H. A. R.: Derivation of an effective height for scintillometers: La Poza experiment in Northwest Mexico, *J. Hydrometeorol.*, 4, 915–928, 2003.
- He, Y., Gao, Z., Guo, T., Qu, F., Liang, D., Li, D., Shi, J., and Shan, B.: Fine particulate matter associated mortality burden of lung cancer in Hebei Province, China, *Thorac. Cancer*, 9, 820–826, <https://doi.org/10.1111/1759-7714.12653>, 2018.
- Hourdin, F., Gueye, M., Diallo, B., Dufresne, J. L., Escribano, J., Menut, L., Marticorena, B., Siour, G., and Guichard, F.: Parameterization of convective transport in the boundary layer and its impact on the representation of the diurnal cycle of wind and dust emissions, *Atmos. Chem. Phys.*, 15, 6775–6788, <https://doi.org/10.5194/acp-15-6775-2015>, 2015.
- Huang, R.-J., Zhang, Y., Bozzetti, C., Ho, K.-F., Cao, J.-J., Han, Y., Daellenbach, K. R., Slowik, J. G., Platt, S. M., Canonaco, F., Zotter, P., Wolf, R., Pieber, S. M., Brun, E. A., Crippa, M., Ciarelli, G., Piazzalunga, A., Schwikowski, M., Abbaszade, G., Schnelle-Kreis, J., Zimmermann, R., An, Z., Szidat, S., Baltensperger, U., El Haddad, I., and Prevot, A. S. H.: High secondary aerosol contribution to particulate pollution during haze events in China, *Nature*, 514, 218–222, <https://doi.org/10.1038/nature13774>, 2014.
- Järvi, L., Rannik, Ü., Mammarella, I., Sogachev, A., Aalto, P. P., Keronen, P., Siivola, E., Kulmala, M., and Vesala, T.: Annual particle flux observations over a heterogeneous urban area, *Atmos. Chem. Phys.*, 9, 7847–7856, <https://doi.org/10.5194/acp-9-7847-2009>, 2009.
- Kaimal, J. C., Izumi, Y., Wyngaard, J. C., and Cote, R.: Spectral characteristics of surface-layer turbulence, *Q. J. R. Meteorol. Soc.*, 98, 563–589, 1972.
- Karvosenoja, N., Tainio, M., Kupiainen, K., Tuomisto, J. T., Kukkonen, J., and Johansson, M.: Evaluation of the emissions and uncertainties of PM<sub>2.5</sub> originated from vehicular traffic and domestic wood combustion in Finland, *Boreal Environ. Res.*, 13, 465–474, 2008.
- Ketzel, M., Wahlin, P., Berkowicz, R., and Palmgren, F.: Particle and trace gas emission factors under urban driving conditions in Copenhagen based on street and roof-level observations, *Atmos. Environ.*, 37, 2735–2749, [https://doi.org/10.1016/s1352-2310\(03\)00245-0](https://doi.org/10.1016/s1352-2310(03)00245-0), 2003.
- Krecl, P., Targino, A. C., Landi, T. P., and Ketzel, M.: Determination of black carbon, PM<sub>2.5</sub>, particle number and NO<sub>x</sub> emission factors from roadside measurements and their implications for emission inventory development, *Atmos. Environ.*, 186, 229–240, <https://doi.org/10.1016/j.atmosenv.2018.05.042>, 2018.
- Lagouarde, J. P., Irvine, M., Bonnefond, J. M., Grimmond, C. S. B., Long, N., Oke, T. R., Salmond, J. A., and Offerle, B.: Monitoring the sensible heat flux over urban areas using large aperture scintillometry: Case study of Marseille city during the escompte experiment, *Bound.-Lay. Meteorol.*, 118, 449–476, <https://doi.org/10.1007/s10546-005-9001-0>, 2006.
- Leclerc, M. Y. and Foken, T.: Footprints in Micrometeorology and Ecology, Springer, Heidelberg, 254 pp., 2014.
- Lee, X.: Handbook of Micrometeorology, A Guide for Surface Flux Measurement and Analysis, edited by: Lee, X., Kluwer academic publishers, New York, USA, 250 pp., 2004.
- Lei, H. and Wuebbles, D. J.: Chemical competition in nitrate and sulfate formations and its effect on air quality, *Atmos. Environ.*, 80, 472–477, <https://doi.org/10.1016/j.atmosenv.2013.08.036>, 2013.
- Li, J., Sun, J., Zhou, M., Cheng, Z., Li, Q., Cao, X., and Zhang, J.: Observational analyses of dramatic developments of a severe air pollution event in the Beijing area, *Atmos. Chem. Phys.*, 18, 3919–3935, <https://doi.org/10.5194/acp-18-3919-2018>, 2018.
- Li, M., Liu, H., Geng, G., Hong, C., Liu, F., Song, Y., Tong, D., Zheng, B., Cui, H., Man, H., Zhang, Q., and He, K.: Anthropogenic emission inventories in China: a review, *Natl. Sci. Rev.*, 4, 834–866, <https://doi.org/10.1093/nsr/nwx150>, 2017.
- Li, Q.-C., Li, J., Zheng, Z.-F., Wang, Y.-T., and Yu, M.: Influence of mountain valley breeze and sea land breeze in winter on distribution of air pollutants in Beijing-tianjin-hebei region, *Environ. Sci. Technol.*, 40, 513–524, 2019.
- Li, X., Hu, F., and Shu, W.: Study on the characteristics of winter island heat islands in Beijing and the influence factors of strong and weak heat islands, *Journal of the Graduate School of the Chinese Academy of Sciences*, 4, 431–438, 2007.
- Liu, H., Man, H., Cui, H., Wang, Y., Deng, F., Wang, Y., Yang, X., Xiao, Q., Zhang, Q., Ding, Y., and He, K.: An updated emission inventory of vehicular VOCs and IVOCs in China, *Atmos. Chem. Phys.*, 17, 12709–12724, <https://doi.org/10.5194/acp-17-12709-2017>, 2017.
- Lou, S., Liao, H., and Zhu, B.: Impacts of aerosols on surface-layer ozone concentrations in China through heterogeneous reactions and changes in photolysis rates, *Atmos. Environ.*, 85, 123–138, <https://doi.org/10.1016/j.atmosenv.2013.12.004>, 2014.
- Lu, Z., Zhang, Q., and Streets, D. G.: Sulfur dioxide and primary carbonaceous aerosol emissions in China and India, 1996–2010, *Atmos. Chem. Phys.*, 11, 9839–9864, <https://doi.org/10.5194/acp-11-9839-2011>, 2011.
- Mårtensson, E. M., Nilsson, E. D., Buzorius, G., and Johansson, C.: Eddy covariance measurements and parameterisation of traffic related particle emissions in an urban environment, *Atmos. Chem. Phys.*, 6, 769–785, <https://doi.org/10.5194/acp-6-769-2006>, 2006.
- Mayol, E., Jimenez, M. A., Herndl, G. J., Duarte, C. M., and Arrieta, J. M.: Resolving the abundance and air-sea fluxes of airborne microorganisms in the North Atlantic Ocean, *Front. Microbiol.*, 5, 557, <https://doi.org/10.3389/fmicb.2014.00557>, 2014.
- MEP, P. R. C.: Technical regulation on ambient air quality index, Ministry of Environmental Protection, Beijing, 12 pp., 2012.
- Moene, A. F., Beyrich, F., and Hartogensis, O. K.: Developments in scintillometry, *B. Am. Meteorol. Soc.*, 90, 694–698, <https://doi.org/10.1175/2008bams2672.1>, 2009.
- Nebuloni, R.: Empirical relationships between extinction coefficient and visibility in fog, *Appl. Opt.*, 44, 3795–3804, 10.1364/ao.44.003795, 2005.
- Nemitz, E., Dorsey, J. R., Flynn, M. J., Gallagher, M. W., Hensen, A., Erisman, J.-W., Owen, S. M., Dämmgen, U., and Sutton, M. A.: Aerosol fluxes and particle growth above managed grassland, *Biogeosciences*, 6, 1627–1645, <https://doi.org/10.5194/bg-6-1627-2009>, 2009.
- Ripamonti, G., Jarvi, L., Molgaard, B., Hussein, T., Nordbo, A., and Hameri, K.: The effect of local sources on aerosol particle number size distribution, concentrations and fluxes in Helsinki, Finland, *Tellus B*, 65, 19786, <https://doi.org/10.3402/tellusb.v65i0.19786>, 2013.

- Roden, C. A., Bond, T. C., Conway, S., Benjamin, A., and Pinel, O.: Emission factors and real-time optical properties of particles emitted from traditional wood burning cookstoves, *Environ. Sci. Technol.*, 40, 6750–6757, <https://doi.org/10.1021/es052080i>, 2006.
- Shen, G., Tao, S., Wei, S., Chen, Y., Zhang, Y., Shen, H., Huang, Y., Zhu, D., Yuan, C., Wang, H., Wang, Y., Pei, L., Liao, Y., Duan, Y., Wang, B., Wang, R., Lv, Y., Li, W., Wang, X., and Zheng, X.: Field Measurement of Emission Factors of PM, EC, OC, Parent, Nitro-, and Oxy- Polycyclic Aromatic Hydrocarbons for Residential Briquette, Coal Cake, and Wood in Rural Shanxi, China, *Environ. Sci. Technol.*, 47, 2998–3005, <https://doi.org/10.1021/es304599g>, 2013.
- Shen, X., Sun, J., Zhang, X., Zhang, Y., Wang, Y., Tan, K., Wang, P., Zhang, L., Qi, X., Che, H., Zhang, Z., Zhong, J., Zhao, H., and Ren, S.: Comparison of Submicron Particles at a Rural and an Urban Site in the North China Plain during the December 2016 Heavy Pollution Episodes, *J. Meteorol. Res.*, 32, 26–37, <https://doi.org/10.1007/s13351-018-7060-7>, 2018.
- Sproson, D. A. J., Brooks, I. M., and Norris, S. J.: The effect of hygroscopicity on eddy covariance estimates of sea-spray aerosol fluxes: a comparison of high-rate and bulk correction methods, *Atmos. Meas. Tech.*, 6, 323–335, <https://doi.org/10.5194/amt-6-323-2013>, 2013.
- Stull, R. B.: *An Introduction to Boundary Layer Meteorology*, Reidel Publishing Co., Dordrecht, 666 pp., 1988.
- Su, F., Gao, Q., Zhang, Z., REN, Z.-H., and YANG, X.-X.: Transport pathways of pollutants from outside in atmosphere boundary layer, *Res. Environ. Sci.*, 1, 26–29, <https://doi.org/10.13198/j.res.2004.01.28.sufq.005>, 2004.
- Sun, Y., Jiang, Q., Wang, Z., Fu, P., Li, J., Yang, T., and Yin, Y.: Investigation of the sources and evolution processes of severe haze pollution in Beijing in January 2013, *J. Geophys. Res.-Atmos.*, 119, 4380–4398, <https://doi.org/10.1002/2014jd021641>, 2014.
- Tatarskii, V. I.: *Wave Propagation in a Turbulent Medium*, McGraw-Hill Book Company Inc., New York, 285 pp., 1961.
- Vogt, M., Nilsson, E. D., Ahlm, L., Martensson, E. M., and Johansson, C.: Seasonal and diurnal cycles of 0.25–2.5  $\mu\text{m}$  aerosol fluxes over urban Stockholm, Sweden, *Tellus B*, 63, 935–951, <https://doi.org/10.1111/j.1600-0889.2011.00551.x>, 2011a.
- Vogt, M., Nilsson, E. D., Ahlm, L., Martensson, E. M., and Johansson, C.: The relationship between 0.25–2.5  $\mu\text{m}$  aerosol and  $\text{CO}_2$  emissions over a city, *Atmos. Chem. Phys.*, 11, 4851–4859, <https://doi.org/10.5194/acp-11-4851-2011>, 2011b.
- Wang, H., Lu, K., Chen, X., Zhu, Q., Wu, Z., Wu, Y., and Sun, K.: Fast particulate nitrate formation via  $\text{N}_2\text{O}_5$  uptake aloft in winter in Beijing, *Atmos. Chem. Phys.*, 18, 10483–10495, <https://doi.org/10.5194/acp-18-10483-2018>, 2018.
- Wang, Y. H., Liu, Z. R., Zhang, J. K., Hu, B., Ji, D. S., Yu, Y. C., and Wang, Y. S.: Aerosol physicochemical properties and implications for visibility during an intense haze episode during winter in Beijing, *Atmos. Chem. Phys.*, 15, 3205–3215, <https://doi.org/10.5194/acp-15-3205-2015>, 2015.
- Wang, Z., Li, J., Wang, Z., Yang, W., Tang, X., Ge, B., Yan, P., Zhu, L., Chen, X., Chen, H., Wand, W., Li, J., Liu, B., Wang, X., Wand, W., Zhao, Y., Lu, N., and Su, D.: Modeling study of regional severe hazes over mid-eastern China in January 2013 and its implications on pollution prevention and control, *Sci. China-Earth Sci.*, 57, 3–13, <https://doi.org/10.1007/s11430-013-4793-0>, 2014.
- Whitehead, J. D., Gallagher, M. W., Dorsey, J. R., Robinson, N., Gabey, A. M., Coe, H., McFiggans, G., Flynn, M. J., Ryder, J., Nemitz, E., and Davies, F.: Aerosol fluxes and dynamics within and above a tropical rainforest in South-East Asia, *Atmos. Chem. Phys.*, 10, 9369–9382, <https://doi.org/10.5194/acp-10-9369-2010>, 2010.
- Wu, Q., Wang, Z., Chen, H., Zhou, W., and Wenig, M.: An evaluation of air quality modeling over the Pearl River Delta during November 2006, *Meteorol. Atmos. Phys.*, 116, 113–132, <https://doi.org/10.1007/s00703-011-0179-z>, 2012.
- Wyngaard, J. C.: *Turbulence in the Atmosphere*, Cambridge University Press, New York, 393 pp., 2010.
- Wyngaard, J. C., Izumi, Y., and Collins, S. A.: Behavior of refractive-index-structure parameter near ground, *J. Opt. Soc. Am.*, 61, 1646–1650, <https://doi.org/10.1364/josa.61.001646>, 1971.
- Yuan, R., Luo, T., Sun, J., Zeng, Z., Ge, C., and Fu, Y.: A new method for measuring the imaginary part of the atmospheric refractive index structure parameter in the urban surface layer, *Atmos. Chem. Phys.*, 15, 2521–2531, <https://doi.org/10.5194/acp-15-2521-2015>, 2015.
- Yuan, R., Luo, T., Sun, J., Liu, H., Fu, Y., and Wang, Z.: A new method for estimating aerosol mass flux in the urban surface layer using LAS technology, *Atmos. Meas. Tech.*, 9, 1925–1937, <https://doi.org/10.5194/amt-9-1925-2016>, 2016.
- Zeweldi, D. A., Gebremichael, M., Wang, J., Sammis, T., Kleissl, J., and Miller, D.: Intercomparison of Sensible Heat Flux from Large Aperture Scintillometer and Eddy Covariance Methods: Field Experiment over a Homogeneous Semi-arid Region, Bound.-Lay. Meteorol., 135, 151–159, <https://doi.org/10.1007/s10546-009-9460-9>, 2010.
- Zhang, H. and Li, X.: Review of the field measurements and parameterization for dust emission during sand-dust events, *J. Meteorol. Res.*, 28, 903–922, <https://doi.org/10.1007/s13351-014-3296-z>, 2014.
- Zhang, Q., Streets, D. G., Carmichael, G. R., He, K. B., Huo, H., Kannari, A., Klimont, Z., Park, I. S., Reddy, S., Fu, J. S., Chen, D., Duan, L., Lei, Y., Wang, L. T., and Yao, Z. L.: Asian emissions in 2006 for the NASA INTEX-B mission, *Atmos. Chem. Phys.*, 9, 5131–5153, <https://doi.org/10.5194/acp-9-5131-2009>, 2009a.
- Zhang, X., Zhong, J., Wang, J., Wang, Y., and Liu, Y.: The interdecadal worsening of weather conditions affecting aerosol pollution in the Beijing area in relation to climate warming, *Atmos. Chem. Phys.*, 18, 5991–5999, <https://doi.org/10.5194/acp-18-5991-2018>, 2018.
- Zhang, X. Y., Wang, Y. Q., Lin, W. L., Zhang, Y. M., Zhang, X. C., Gong, S., Zhao, P., Yang, Y. Q., Wang, J. Z., Hou, Q., Zhang, X. L., Che, H. Z., Guo, J. P., and Li, Y.: Changes of Atmospheric Composition and Optical Properties over Beijing 2008 Olympic Monitoring Campaign, *B. Am. Meteorol. Soc.*, 90, 1633–1651, <https://doi.org/10.1175/2009bams2804.1>, 2009b.
- Zhang, X. Y., Wang, Y. Q., Niu, T., Zhang, X. C., Gong, S. L., Zhang, Y. M., and Sun, J. Y.: Atmospheric aerosol compositions in China: spatial/temporal variability, chemical signature, regional haze distribution and comparisons with global aerosols,

- Atmos. Chem. Phys., 12, 779–799, <https://doi.org/10.5194/acp-12-779-2012>, 2012.
- Zhang, Y. and Tao, S.: Global atmospheric emission inventory of polycyclic aromatic hydrocarbons (PAHs) for 2004, Atmos. Environ., 43, 812–819, <https://doi.org/10.1016/j.atmosenv.2008.10.050>, 2009.
- Zheng, B., Zhang, Q., Tong, D., Chen, C., Hong, C., Li, M., Geng, G., Lei, Y., Huo, H., and He, K.: Resolution dependence of uncertainties in gridded emission inventories: a case study in Hebei, China, Atmos. Chem. Phys., 17, 921–933, <https://doi.org/10.5194/acp-17-921-2017>, 2017.
- Zhong, J., Zhang, X., Wang, Y., Sun, J., Zhang, Y., Wang, J., Tan, K., Shen, X., Che, H., and Zhang, L.: Relative contributions of boundary-layer meteorological factors to the explosive growth of PM<sub>2.5</sub> during the red-alert heavy pollution episodes in Beijing in December 2016, J. Meteorol. Res., 31, 809–819, <https://doi.org/10.1007/s13351-017-7088-0>, 2017a.
- Zhong, J., Zhang, X., Wang, Y., Sun, J., Zhang, Y., Wang, J., Tan, K., Shen, X., Che, H., Zhang, L., Zhang, Z., Qi, X., Zhao, H., Ren, S., and Li, Y.: Relative Contributions of Boundary-Layer Meteorological Factors to the Explosive Growth of PM<sub>2.5</sub> during the Red-Alert Heavy Pollution Episodes in Beijing in December 2016, J. Meteorol. Res., 31, 809–819, <https://doi.org/10.1007/s13351-017-7088-0>, 2017b.
- Zhong, J., Zhang, X., Dong, Y., Wang, Y., Liu, C., Wang, J., Zhang, Y., and Che, H.: Feedback effects of boundary-layer meteorological factors on cumulative explosive growth of PM<sub>2.5</sub> during winter heavy pollution episodes in Beijing from 2013 to 2016, Atmos. Chem. Phys., 18, 247–258, <https://doi.org/10.5194/acp-18-247-2018>, 2018a.
- Zhong, J., Zhang, X., Dong, Y., Wang, Y., Liu, C., Wang, J., Zhang, Y., and Che, H.: Feedback effects of boundary-layer meteorological factors on cumulative explosive growth of PM<sub>2.5</sub> during winter heavy pollution episodes in Beijing from 2013 to 2016, Atmos. Chem. Phys., 18, 247–258, <https://doi.org/10.5194/acp-18-247-2018>, 2018b.
- Zhong, J., Zhang, X., Wang, Y., Liu, C., and Dong, Y.: Heavy aerosol pollution episodes in winter Beijing enhanced by radiative cooling effects of aerosols, Atmos. Res., 209, 59–64, <https://doi.org/10.1016/j.atmosres.2018.03.011>, 2018c.
- Zou, J., Liu, G., Sun, J., Zhang, H., and Yuan, R.: The momentum flux-gradient relations derived from field measurements in the urban roughness sublayer in three cities in China, J. Geophys. Res.-Atmos., 120, 10797–10809, <https://doi.org/10.1002/2015jd023909>, 2015.
- Zou, J., Sun, J., Liu, G., Yuan, R., and Zhang, H.: Vertical Variation of the Effects of Atmospheric Stability on Turbulence Statistics Within the Roughness Sublayer Over Real Urban Canopy, J. Geophys. Res.-Atmos., 123, 2017–2036, <https://doi.org/10.1002/2017jd027041>, 2018.